UNIVERSITY of
BRADFORD

Library

The University of Bradford Institutional Repository

http://bradscholars.brad.ac.uk

Steady State and Dynamic Modeling of Spiral Wound Wastewater Reverse Osmosis Process

M. A. Al-Obaidi and I. M. Mujtaba*

School of Engineering, University of Bradford, Bradford, West Yorkshire BD7 1DP, UK
*Corresponding author, Tel.: +44 0 1274 233645
E-mail address: I.M.Mujtaba@bradford.ac.uk, M.A.A.Alobaidi@student.bradford.ac.uk

Abstract

Reverse osmosis (RO)is one of the most important technologies used in wastewater treatment plants due to high contaminant rejection and low utilization of energy in comparison to other treatment procedures. For single-component spiral-wound reverse osmosis membrane process, one dimensional steady state and dynamic mathematical models have been developed based on the solution-diffusion model coupled with the concentration polarization mechanism. The model has been validated against reported data for wastewater treatment from literature at steady state conditions. Detailed simulation using the dynamic model has been carried out in order to gain deeper insight of the process. The effect of feed flow rate, pressure, temperature and concentration of pollutants on the performance of the process measured in terms of salt rejection, recovery ratio and permeate flux has been investigated.

*Keywords***:** Spiral-wound reverse osmosis; One dimensional steady state and dynamic modeling; Wastewater treatment

1. Introduction

Reverse osmosis can be defined as a process of removing undesirable species (salts, pollutants, etc.) from liquid solutions (seawater, wastewater, etc.) by pumping the solution at higher pressure than the osmotic pressure within a closed vessel which facilitates the solvent to flow from the concentrated side to the diluted side (Jain et al., 2004). Over the last decades, the membrane technology has experienced significant advancement that reduces the cost of filtration and enhances the quality of drinking water. As a consequence, this technology can be considered as the lowest cost technology for water desalination (Carter, 2015) in comparison to others existing technologies, such as thermal desalination (multistage flash desalination, MSF; multi-effect distillation, MED) (Moonkhum et al., 2010). RO is a prominent separation process in process industries (such as textile, paper, food, electrochemical, biochemical industries) and in wastewater treatment in addition to water desalination due to its power to separate impurities effectively and in a way appropriate to the

1

environmental demands (Elhalwagi, 1992; Bódalo-Santoyo et al., 2003; Nguyen et al., 2009; Slater et al., 1983). As a result, a number of researchers in the past decades developed several mathematical models of RO desalination process in order to explain the separation technique and to carry out model based optimisation to enhance the efficiency of the production process (Sassi and Mujtaba, 2012, 2013a,b; Barello et al., 2015; Manenti et al., 2015).

In RO process, the solution-diffusion model has been widely considered as one of the simplest non-porous or homogeneous models related to transport mechanism through the membrane (Mujtaba, 2012). Avlonitis et al. (1991, 1993 and 2007) have developed an explicit analytical steady state spatial model for spiral-wound modules based on the solution-diffusion theory but assumed constant physical properties and neglected the diffusive mass transport along the axial and spiral dimensions in both channels. Boudinar et al. (1992) have proposed another steady state model for spiral-wound RO module based on the solution-diffusion model assuming the pressure loss in the two channels being a function of brine and permeate friction parameters (Darcy's law for porous media) and constant fluid density.

A one dimensional steady state model for spiral-wound RO membranes has been developed by Geraldes et al. (2005) based on the solution-diffusion model but including the variation of velocity, pressure and brine concentration along the membrane length with temperature impact. However, the model neglected the pressure drop in the permeate channel and the diffusion flow in the feed side. Sagne et al. (2009) considered a modified unsteady state one dimensional model based on the solution-diffusion model for the rejection of dilute aqueous solution of five volatile organic compounds from brackish water used in fermentation industries. The model neglected the impact of concentration polarization and degraded the flux of solute.

All the above proposed models are validated with the sea water and brackish water experimental data.

Sundaramoorthy et al. (2011a,b) have stated a one dimensional analytical study state model by assuming the validity of the solution-diffusion model and incorporates the spatial variation of pressure, flow rates and solute concentration in the feed channel. Also, the model assumed constant values for both the permeate concentration and pressure along the permeate side and constant temperature. The model has been validated with the experimental data of organic solute but showed an increase in the average permeate concentration due to increase in the operating pressure for most of the mathematical predictions.

In a summary, sea and brackish water desalination have been extensively modelled as one and two dimensional steady state and dynamic models with a number of assumptions (Sirkar

2

et al., 1982; Senthilmurugan et al., 2005). However, a limited number of published models describing RO process, especially for wastewater treatment is available in the public domain (Sundaramoorthy et al., 2011a).In addition, there are a few validation studies of mathematical models with wastewater experimental data (Sundaramoorthy et al., 2011b).

In this work, a one dimensional steady state and dynamic model applicable for spiral-wound RO process is suggested. This model will base on the solution-diffusion model and relax the assumptions of constant physical properties and concentration of the fresh water on the permeate side. In addition, the brine concentration varies along the membrane length due to the impact of both plug-flow and diffusion flow. Also, it will consider the impacts of diffusion, temperature and concentration polarization on the whole process. The robustness of this model will be appraised by a simulation study with an observational data for wastewater treatment from literature. Then, the effect of feed flow rate, pressure, concentration and temperature will be checked on the efficiency of the unit for recovery ratio, salt rejection and permeate flux. Finally, the system response will be checked for different step changes of operating parameters.

2. Model development

2.1 The main principles

Spiral-wound modules contain an envelope of a number of glued flat membranes wrapped around a central tube. The brine water is pumped and forced to run along the membrane length where the fresh water is collected out in the tube at the permeate side. Fig. 1shows the direction of flow inside the module. The specific dimensions of the module are length and width (L and W) and the feed and permeate space channels are (t_f and t_p) [m] respectively with $A_m = LW$ [m²] as the area of the membrane. Also, according to the method of discretization used by $gPROMS$(Process system Enterprise Ltd., 2001),the area of the membrane will be split into four sub-sections of equal area where the proportion of each sub-section will be obtained by:

$A_{section} = W \Delta x$ (1)

Where, $\Delta x = \frac{L}{4}$

Specifically, the reverse osmosis module (Fig. 1) is composed of two sides, the feed side where the brine flow rate changes along (x) (the horizontal direction) and the permeate side. The accumulated permeate water flows in the same direction of feed and then flows in the spiral direction into a central perforated pipe. While, the fresh water is flowing perpendicular

from the feed side to the permeate side through the membrane region. As mentioned above, the model in this work will employ the solution-diffusion model to identify the criteria of separation along the membrane. Besides, the concentration polarization theory will be used to describe the deviation of mass transfer coefficient in the feed channel. The validation of this model will be carried out using experimental data from a laboratory scale spiral-wound RO based wastewater treatment process removing chlorophenol from diluted aqueous solutions. The model will include explicit steady and dynamic equations for calculating the solute concentration on the wall of the membrane, the brine and permeate channels together with the pressure, water and solute fluxes, brine and permeate flow rates and finally the temperature at each point along the one dimension in both sides of the membrane.
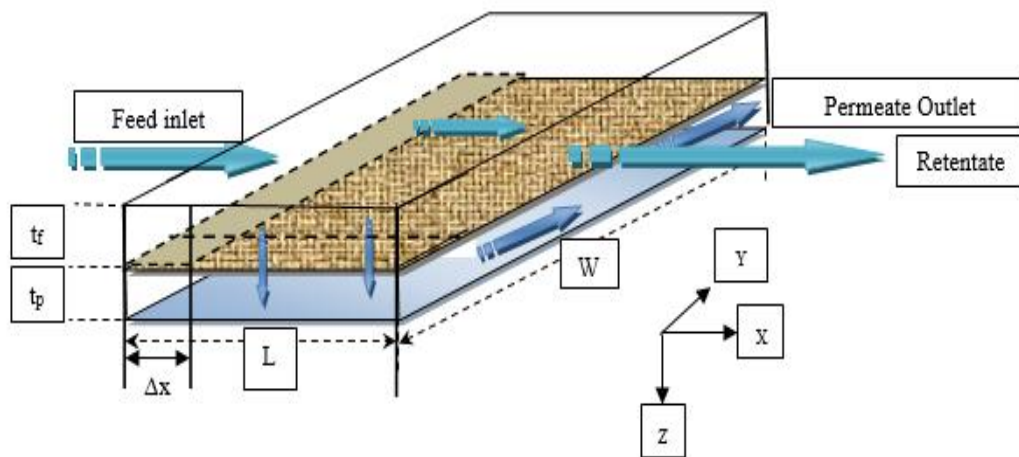

Fig.1: Schematic diagram of a spiral wound membrane module

2.2 The assumptions

The following assumptions were made to develop the process model:

1. Flat membrane sheet with negligible channel curvature.
2. Validity of the solution-diffusion model.
3. Validity of the Darcy's law for the feed channel where the friction parameter is applied to characterize the pressure drop.
4. Negligible pressure drop in the freshwater side and a constant pressure of 1 atm is assumed.
5. The permeate concentration will be varied along the membrane length, but the mean value will be considered as the fresh water output concentration for the calculation of

the whole unit solute rejection. This is attributed to the direction of the accumulated permeate flow rate, which is in the spiral direction.

6. Negligible flow rate in spiral direction for brine channel (one dimensional model).

Note, these assumptions are considered based on the extensive literature review on RO process models considered by others (as referenced in section 1) for desalination. Interestingly as presented in later sections, these assumptions were found to be also quite valid for the considered RO process for wastewater treatment (see section 5).

3. Model structure

According to the principles of the solution-diffusion model which assumes no interaction between the solute and solvent fluxes, the solvent and solute fluxes (J_w and J_s) [m/sec and $Kmol/m^2sec$] through the membrane are (Lonsdale et al., 1965):

$$J_{w(x)} = A_w \left(\Delta P_{b\,(x)} - \Delta \pi_{(x)} \right) \tag{2}$$

$$J_{s(x)} = B_s \left(C_{w(x)} - C_{p(x)} \right) \tag{3}$$

Where, A_w [$m/atm\ sec$] and B_s [m/sec] are the pure water and solute permeability constants of the membrane. ($\Delta P_b - \Delta \pi$) [atm] is the quantity of force per unit area required to cope with the osmotic pressure and to release pure water from the feed solution. ΔP is the trans-membrane pressure and $\Delta \pi$ is the osmotic pressure difference along the length of the membrane L [m] defined by Eqs. (4 and 5). (C_w, C_p) [$Kmol/m^3$] are the solute concentration at the membrane wall and permeate side respectively.

$$\Delta P_{b\,(x)} = \left(P_{b(x)} - P_p \right)$$

(4)

$$\Delta \pi_{(x)} = RT_{b(x)} \left(C_{w(x)} - C_{p(x)} \right) \tag{5}$$

Where, R, T_b, P_b and P_p [$atm\ m^3/KmolK,\ K$ and atm] are the gas constant, the temperature of the brine, the brine pressure and the permeate pressure respectively.

J_w is linked to concentration polarization and k [m/sec] (mass transfer coefficient of the solute through the membrane) by the following equation:

$$\frac{(C_{w(x)} - C_{p(x)})}{(C_{b(x)} - C_{p(x)})} = exp \left(\frac{J_{w(x)}}{k_{(x)}} \right) \tag{6}$$

With 100% of solute rejection ($C_{p(x)} = 0$), the above equation reduces to:

$$\frac{(C_{w(x)})}{(C_{b(x)})} = exp \left(\frac{J_{w(x)}}{k_{(x)}} \right) \tag{7}$$

Where, $C_{w(x)}$ and $C_{b(x)}$ [$Kmol/m^3$] are the solute concentration at the wall of membrane and brine channel respectively.

By substituting Eqs. (4 and 5) in Eq. (2) and Eq. (6) in Eq. (3), it gives:

$$J_{w(x)} = A_w \left((P_{b(x)} - P_p) - RT_{b(x)}(C_{w(x)} - C_{p(x)}) \right) \quad (8)$$

$$J_{s(x)} = B_s \, exp\left(\frac{J_{w(x)}}{k_{(x)}}\right)(C_{b(x)} - C_{p(x)}) \quad (9)$$

Also, the solute flux through the membrane can be written as:

$$J_{s(x)} = J_{w(x)} C_{p(x)} \quad (10)$$

The total (whole module) mass and solute balance can be presented as:

$$\frac{F_{b(0)} \, \rho_{b(0)}}{M_{wb(0)}} = \frac{F_{b(x)} \, \rho_{b(x)}}{M_{wb(x)}} + \frac{F_{p(x)} \, \rho_{p(x)}}{M_{wp(x)}} \quad (11)$$

Where, $F_{b(0)}$, $\rho_{b(0)}$, $F_{b(x)}$, $\rho_{b(x)}$, $F_{p(x)}$ and $\rho_{p(x)}$ [m^3/sec, Kg/m^3] are the feed flow rate and density at ($x=0$) any point along the feed and permeate channels respectively.

By assuming constant density and molecular weight (due to small quantity of contaminant), Eq. (11) can be written as:

$$F_{b(0)} = F_{b(x)} + F_{p(x)} \quad (12)$$

$$F_{b(0)} C_{b(0)} = F_{b(x)} C_{b(x)} + F_{p(x)} C_{p(x)} \quad (13)$$

The change in brine flow rate in (x) direction can be estimated with the water flux through the membrane, by using:

$$\frac{dF_{b(x)}}{dx} = -\frac{dF_{p(x)}}{dx} = -W J_{w(x)} \quad (14)$$

Similarly, the permeate flow rate for each sub-section can be written as:

$$F_{p(x)} = J_{w(x)} W \Delta x \quad (15)$$

Where, Δx [m] is the length of the sub-section.

Finally, the pressure drop along the length of the membrane in the brine channel can be accounted from the momentum balance equation which is based on the Darcy's law where the pressure loss is caused by the wall friction along the membrane:

$$\frac{dP_{b(x)}}{dx} = -b F_{b(x)} \quad (16)$$

Where, b [$atm \, sec/m^4$] is the friction factor along the feed and permeate channels.

3.1 The conservation equations of the dynamic model

One of the requirements for designing control systems of RO is the development of a dynamic model which can predict the transient characteristics of the plant and be used later to

maintain an acceptable level of cost. The brine concentration varies along the membrane length due to the impact of the plug-flow and diffusion terms.

According to solute balance along (*x-axis*) of membrane length and for sub-section of (Δx), the change of solute hold-up can be written as:

$$\frac{d(C_{b(x)}W\,t_f\,\Delta x)}{dt} = \left(F_s\,W\,t_f\right)_{x=0} - \left(F_s\,W\,t_f\right)_{x=\Delta x} - J_{s(x)}\,W\,\Delta x \quad (17)$$

Where, F_s [*Kmol/m² sec*] is the solute molar flux in *x*-direction and J_s [*Kmol/m² sec*] is the solute molar flux through the membrane. By dividing the two sides of the above equation by the volume of sub-section with an arrangement, it reduces to:

$$\frac{d(C_{b(x)})}{dt} = -\left[\frac{(F_s)_{x=\Delta x}-(F_s)_{x=0}}{\Delta x}\right] - \frac{J_{s(x)}}{t_f}(18)$$

$$\frac{d(C_{b(x)})}{dt} = -\left[\frac{dF_{s(x)}}{\Delta x}\right] - \frac{J_{s(x)}}{t_f} \quad (19)$$

The solute molar flux can be defined as:

$$F_{s(x)} = \frac{C_{b(x)}\,F_{b(x)}}{W\,t_f} - D_{b(x)}\frac{dC_{b(x)}}{dx} \quad (20)$$

Where, $D_{b(x)}$ [*m²/sec*] is the diffusivity coefficient of brine in water. The second term of Eq. (20) explains the effect of dispersion flux in the bulk fluid.

Finally, the set of dynamic model equations for the brine and permeate concentrations can be written as:

$$\frac{dC_{b(x)}}{dt} = -\frac{C_{b(x)}}{t_f\,W}\frac{dF_{b(x)}}{dx} - \frac{F_{b(x)}}{t_f\,W}\frac{dC_{b(x)}}{dx} + \frac{d}{dx}\left[D_{b(x)}\frac{dC_{b(x)}}{dx}\right] - \frac{J_{w(x)}C_{p(x)}}{t_f} \quad (21)$$

Similarly, for the permeate concentration:

$$\frac{dC_{p(x)}}{dt} = -\frac{C_{p(x)}}{t_p\,W}\frac{dF_{p(x)}}{dx} - \frac{F_{p(x)}}{t_p\,W}\frac{dC_{p(x)}}{dx} + \frac{d}{dx}\left[D_{p(x)}\frac{dC_{p(x)}}{dx}\right] + \frac{J_{w(x)}C_{p(x)}}{t_f} \quad (22)$$

Where, D_p [*m²/sec*] is the diffusivity coefficient of permeate along the length of the membrane which varies with temperature and concentration.

As can be seen from the above two equations, the dynamic behaviour of both feed and permeate concentrations is controlled by the flux of solute penetrate the membrane. Also, the dynamic behaviour of brine flow rate, brine and permeate pressures can be estimated from Eqs. (14 and 16):

$$\frac{dF_{b(x)}}{dt} = \left[\left\{-W\left(A_w\left((P_{b(x)}-P_p) - R\,T_{b(x)}\,exp\left(\frac{J_{w(x)}}{k_{(x)}}\right)\left(C_{b(x)}-C_{p(x)}\right)\right)\right)\right\} - \frac{dF_{b(x)}}{dx}\right]\left(\frac{F_{b(x)}}{t_f\,W}\right)(23)$$

$$\frac{dP_{b(x)}}{dt} = \left[\left\{(-b\,F_{b(x)})\right\} - \frac{dP_{b(x)}}{dx}\right]\left(\frac{F_{b(x)}}{t_f\,W}\right) \quad (24)$$

Furthermore, the water and solute fluxes through the membrane can be calculated from:

$$\frac{dJ_{w(x)}}{dt} = \left\{\left(A_w\left((P_{b(x)} - P_p) - RT_{b(x)}(C_{w(x)} - C_{p(x)})\right)\right) - J_{w(x)}\right\}\left(\frac{F_{b(x)}}{t_f\,W\,\Delta x}\right) (25)$$

$$\frac{dJ_{s(x)}}{dt} = \left\{\left(B_s exp\left(\frac{J_{w(x)}}{k_{(x)}}\right)(C_{b(x)} - C_{p(x)})\right) - J_{s(x)}\right\}\left(\frac{F_{b(x)}}{t_f\,W\,\Delta x}\right) \quad (26)$$

The accumulated wall concentration along the length of the membrane can be calculated from:

$$\frac{dC_{w(x)}}{dt} = \left\{\left(C_{p(x)} + exp\left(\frac{J_{w(x)}}{k_{(x)}}\right)(C_{b(x)} - C_{p(x)})\right) - C_{w(x)}\right\}\left(\frac{F_{b(x)}}{t_f\,W\,\Delta x}\right) \quad (27)$$

The last set of equations contains the energy balance dynamic equations of brine and permeate temperatures along the length of the membrane. By assuming well insulated system:

$$\frac{dT_{b(x)}}{dt} = \left[\frac{F_{b(x)}(T_{b(x-\Delta x)} - T_{b(x)})}{t_f\,W\,\Delta x}\right] - \left[\frac{J_{w(x)}(T_{b(x)} - T_{p(x)})}{t_f}\right] (28)$$

$$\frac{dT_{p(x)}}{dt} = \left[\frac{J_{w(x)}(T_{b(x)} - T_{p(x)})}{t_f}\right] \quad (29)$$

Where, T_b and T_p [$°C$] are the temperature at brine and permeate channels respectively.

Occasionally, the values of average solute rejection, the recovery, the total recovery and permeate flow rate at each point and overall permeate flow rate values are calculated as follows:

$$Rej_{(av)} = \frac{C_{b(x=L)} - C_{p(av)}}{C_{b(x=L)}}\,x100 \quad (30)$$

Where, $C_{b(x=L)}$ and $C_{p(av)}$ are the outlet brine and average permeate concentrations respectively.

$$C_{p(av)} = \sum C_{p(x)} \ldots\ldots\ldots\ldots\ldots\ldots\ldots (x = 0\ to\ x = L)(31)$$

$$Rec_{(x)} = \frac{F_{p(x)}}{F_{b(0)}}\,x100 \quad (32)$$

$$Rec_{(Total)} = \frac{F_{p(Total)}}{F_{b(0)}}\,x100 \quad (33)$$

Where, $Rec_{(x)}$ and $Rec_{(Total)}$ are the recovery rate at each point along the brine channel and the total recovery of the whole unit, while $F_{p(x)}$ and $F_{b(0)}$ are the permeate flow rate at each point on the membrane and the inlet feed flow rate respectively.

$$F_{p(x)} = J_{w(x)}\,W\,\Delta x \quad (34)$$

$$F_{p(Total)} = \sum F_{p(x)} \ldots\ldots\ldots\ldots\ldots\ldots (x = 0\ to\ x = L) \quad (35)$$

3.2 The conservation equations of steady-state model

The brine and permeate concentration along the length of the membrane can be estimated by eliminating the hold-up term in the dynamic model Eqs. (21 and 22) and re-arrangement yields:

$$0 = -\frac{C_{b(x)}}{t_f\,W}\frac{dF_{b(x)}}{dx} - \frac{F_{b(x)}}{t_f.W}\frac{dC_{b(x)}}{dx} + \frac{d}{dx}\left[D_{b(x)}\frac{dC_{b(x)}}{dx}\right] - \frac{J_{w(x)}C_{p(x)}}{t_f} \qquad (36)$$

$$0 = -\frac{C_{p(x)}}{t_p\,W}\frac{dF_{p(x)}}{dx} - \frac{F_{p(x)}}{t_p.W}\frac{dC_{p(x)}}{dx} + \frac{d}{dx}\left[D_{p(x)}\frac{dC_{p(x)}}{dx}\right] + \frac{J_{w(x)}C_{p(x)}}{t_f}(37)$$

Eqs. (36 and 37) can be re-written as:

$$\frac{d\frac{(C_{b(x)}F_{b(x)})}{t_f\,W}}{dx} = -\frac{J_{s(x)}}{t_f} + \frac{d}{dx}\left(D_{b(x)}\frac{dC_{b(x)}}{dx}\right) \qquad (38)$$

$$\frac{d\frac{(C_{p(x)}F_{p(x)})}{t_p\,W}}{dx} = \frac{J_{s(x)}}{t_f} + \frac{d}{dx}\left(D_{p(x)}\frac{dC_{p(x)}}{dx}\right) \qquad (39)$$

In addition, the energy balance equations (assuming a constant heat capacity for permeate and brine) for the brine channel can be written as:

$$F_{b(x)}\left(T_{b(x-\Delta x)} - T_{b(x)}\right) = J_{w(x)}\left(T_{b(x)} - T_{p(x)}\right) W\,\Delta x \qquad (40$$

$$\left(T_{b(x)} - T_{p(x)}\right) = 0 \qquad (41)$$

3.3 The physical properties equations

This study covers the experimental work of dilute chlorophenol aqueous solutions on spiral-wound module, so the physical properties equations of the solution has been conceived as identical to water equations. The mass transfer coefficient is a function of pressure, concentration, flow rate and temperature, which means that k will vary with the membrane length. The set of physical properties equations is:

The diffusivity of brine and permeate [m^2/sec] are given by the relations (Koroneos, 2007):

$$D_{b(x)} = 6.725E - 6\ exp\left\{0.1546E - 3\ C_{b(x)}\ x18.01253 - \frac{2513}{T_{b(x)}+273.15}\right\} \qquad (42)$$

$$D_{p(x)} = 6.725E - 6\ exp\left\{0.1546E - 3\ C_{p(x)}x18.01253 - \frac{2513}{T_{p(x)}+273.15}\right\} \qquad (43)$$

While the viscosity of brine and permeate [$Kg/m\ sec$] are given by the relations:

$$\mu_{b(x)} = 1.234E - 6\ exp\left\{0.0212E - 3\ C_{b(x)}\ x18.0153 + \frac{1965}{T_{b(x)}+273.15}\right\} \qquad (44)$$

$$\mu_{p(x)} = 1.234E - 6\ exp\left\{0.0212E - 3\ C_{p(x)}x18.0153 + \frac{1965}{T_{p(x)}+273.15}\right\} \qquad (45)$$

The density of brine and permeate [Kg/m^3] are given by the equations below:

$$\rho_{b(x)} = 498.4 \, m_{f(x)} + \sqrt{\left[248400 \, m_{f(x)}^2 + 752.4 \, m_{f(x)} C_{b(x)} x 18.0153\right]} \quad (46)$$

$$\rho_{p(x)} = 498.4 \, m_{p(x)} + \sqrt{\left[248400 \, m_{p(x)}^2 + 752.4 \, m_{p(x)} C_{p(x)} x 18.0153\right]} \quad (47)$$

Where:

$$m_{f(x)} = 1.0069 - 2.757E - 4 \, T_{b(x)} \qquad\qquad (48)$$

$$m_{p(x)} = 1.0069 - 2.757E - 4 \, T_{p(x)} \qquad\qquad (49)$$

The Reynolds number along the feed and permeate channels can be calculated from:

$$Re_{b(x)} = \frac{\rho_{b(x)} de_b \, F_{b(x)}}{t_f \, W \, \mu_{b(x)}} \qquad\qquad (50)$$

$$Re_{p(x)} = \frac{\rho_{p(x)} de_p \, J_{w(x)}}{\mu_{p(x)}} \qquad\qquad (51)$$

Where, de_b, de_p [m] are the equivalent diameters of the feed and permeate channels respectively.

$$de_b = 2t_f \qquad (52)$$

$$de_p = 2t_p \qquad (53)$$

Finally, the mass transfer coefficient [m/sec] along the feed channel side can be calculated from:

$$k_{(x)} de_b = 147.4 \, D_{b(x)} \, Re_{b(x)}^{0.13} Re_{p(x)}^{0.739} C_{m(x)}^{0.135} \qquad\qquad (54)$$

Where the exponents in Eq. (54) have been experimentally predicted by Sundaramoorthy et al. (2011b) for chlorophenol aqueous solution and showed a fit about 0.99 as a regression coefficient in the method of least squares. Also, C_m is a dimensionless solute concentration and can be calculated from:

$$C_{m(x)} = \frac{C_{b(x)}}{\rho_w} \qquad\qquad (55)$$

Where, ρ_w is the molal density of water (55.56 kmol/m^3).

The final set of model equations used for simulation is presented in Appendix (A) with the degree of freedom analysis.

The model presented in this section is built within gPROMS (**g**eneral **P**rocess **M**odelling **S**ystem) Model builder which provides a modelling platform for steady state and dynamic simulation, optimisation, experiment design and parameter estimation of any process.

4. Problem specifications: Steady-state simulation

The input data satisfying the degree of freedom is shown in Table 1. A commercial thin film composite RO membrane packed into a spiral-wound module (Make: Ion Exchange, India) used by Sundaramoorthy et al. (2011b)in their experimental work to remove chlorophenol from aqueous solutions of different concentrations. The characteristics of the spiral-wound module are presented in Table 1. The transport parameters of this model (A_w, B_s and b) are also shown in Table 1. The solute concentrations vary from(0.778E-3to 6.226E-3$Kmol/m^3$). The feed was pumped in three different flow rates of (2.166E-4, 2.33E-4 and 2.583E-4m^3/sec) with a set of pressures variesfrom5.83 to 13.58 atm for each flow rate.

Table 1
Input data: Membrane characteristics and geometry

Make	Ion Exchange, India
Membrane material	TFC Polyamide
Module configuration	Spiral wound
Number of turns	30
Feed spacer thickness (t_f)	0.8 mm
Permeate channel thickness (t_p)	0.5 mm
Module length (L)	0.934 m
Module width (W)	8.4 m
Module diameter	3.25 $inches$
b	8529.45$\left(\frac{atm.sec}{m^4}\right)$
A_w	9.5188E-7$\left(\frac{m}{atm.sec}\right)$
B_s(chlorophenol)	8.468E-8$\left(\frac{m}{sec}\right)$

5. Model validation

Tables 2, 3 and 4 depict the experimental results of chlorophenol removal carried out by Sundaramoorthy et al. (2011b) and the model predictions for three groups of feed flow rates (each group holding five different feed concentrations under four different feed pressures) with estimated percentage error between the experimental results and the model predictions. Also, Tables 2, 3 and 4 compare the experimental results and the model prediction for the outlet brine concentration, outlet feed flow rate, average permeate concentration and solute rejection with different inlet feed flow rates, pressures and concentrations. As can be seen,

the predicted values of the theoretical model are in a good agreement with experimental ones over the ranges of pressure and concentration. It can be mentioned that the model tends to only underestimate the outlet permeate concentration for lower values of inlet concentration. Apparently, this may be attributed to negligible bulk flow in the spiral direction of the unit. The model is then used for further simulation as reported in the next section. Note that to ensure grid independent solutions 8 zone distributed model has also been tested, but the solutions remained the same as those with 4 zone discretization.

Table 2

Model validation with experimental results for inlet feed flow rate of $(F_b(0) =2.166\text{E-4} m^3/sec)$

No	$P_b(0)$, atm	$T_b(0)$, °C	$C_b(0)E+3$ (Kmol/m³)	$C_b(L)E+3$ (Kmol/m³)		%Error	$C_p(av)E+3$ (Kmol/m³)		%Error	% Rej_{av}		%Error	$F_b(L)E+4$ (m³/sec)		%Error
				Exp.	Model		Exp.	Model		Exp.	Model		Exp.	Model	
1	5.83	30	0.778	0.854	0.8502	0.50	0.37	0.393	-6.21	56.7	53.76	5.18	1.80	1.888	-4.88
2	7.77	30	0.778	0.9042	0.901	0.35	0.368	0.3759	-2.14	59.3	57.8	2.52	1.67	1.754	-5.02
3	9.71	30	0.778	0.948	0.935	1.33	0.366	0.375	-2.45	61.4	59.89	2.45	1.59	1.620	-1.88
4	11.64	30	0.778	1.002	0.983	1.96	0.363	0.3813	-5.04	63.8	61.24	4.01	1.50	1.489	0.73
5	13.58	30	0.778	1.065	1.036	2.73	0.36	0.391	-8.61	66.2	62.27	5.93	1.37	1.357	0.94
6	5.83	32	1.556	1.711	1.723	-0.68	0.652	0.696	-6.74	61.9	59.57	3.76	1.906	1.896	0.52
7	7.77	32	1.556	1.778	1.823	-2.50	0.642	0.635	1.09	63.9	65.18	-2.00	1.736	1.764	-1.61
8	9.71	32	1.556	1.850	1.936	-4.62	0.631	0.613	2.85	65.9	68.34	-3.70	1.63	1.632	-0.14
9	11.64	32	1.556	1.943	2.064	-6.17	0.624	0.6086	2.46	67.9	70.51	-3.84	1.523	1.502	1.33
10	13.58	32	1.556	2.05	2.209	-7.75	0.615	0.6136	0.22	70.0	72.22	-3.17	1.416	1.3737	2.98
11	5.83	32	2.335	2.575	2.58	-0.17	0.886	0.94	-6.09	65.6	63.25	3.58	1.868	1.906	-2.03
12	7.77	32	2.335	2.662	2.73	-2.53	0.884	0.852	3.619	66.8	68.81	-3.00	1.761	1.777	-0.90
13	9.71	32	2.335	2.791	2.9	-3.90	0.882	0.814	7.70	68.4	71.95	-5.19	1.666	1.649	1.02
14	11.64	32	2.335	2.894	3.09	-6.74	0.88	0.801	8.97	69.6	74.11	-6.47	1.566	1.523	2.74
15	13.58	32	2.335	3.044	3.31	-8.70	0.88	0.802	8.86	71.1	75.78	-6.58	1.478	1.398	5.41
16	5.83	32	3.891	4.245	4.268	-0.54	1.244	1.18	5.14	70.7	72.35	-2.33	1.898	1.925	-1.42
17	7.77	32	3.891	4.444	4.525	-1.82	1.231	1.24	-0.73	72.3	72.59	-0.40	1.808	1.800	0.44
18	9.71	32	3.891	4.590	4.801	-4.59	1.299	1.17	9.93	71.7	75.68	-5.55	1.681	1.677	0.23
19	11.64	32	3.891	4.753	5.111	-7.51	1.198	1.14	4.84	74.8	77.78	-3.98	1.65	1.557	5.63
20	13.58	32	3.891	5.029	5.46	-8.55	1.187	1.126	5.13	76.4	79.38	-3.90	1.536	1.437	6.44
21	5.83	31	6.226	6.80	6.75	0.85	1.668	1.82	-9.11	75.5	73.08	3.20	1.923	1.951	-1.47
22	7.77	31	6.226	7.111	7.105	0.09	1.657	1.59	4.04	76.7	77.55	-1.10	1.828	1.838	-0.54
23	9.71	31	6.226	7.381	7.495	-1.54	1.491	1.495	-0.26	79.8	80.05	-0.31	1.75	1.726	1.37
24	11.64	31	6.226	7.763	7.928	-2.12	1.475	1.451	1.62	81.0	81.69	-0.85	1.641	1.615	1.58
25	13.58	31	6.226	8.049	8.411	-4.48	1.457	1.436	1.44	81.9	82.92	-1.24	1.575	1.506	4.38

Table 3

Model validation with experimental results for inlet feed flow rate of ($F_b(0)$ =2.33E-4 m^3/sec)

No	$P_b(0)$, atm	$T_b(0)$, °C	$C_b(0)$E+3 ($Kmol/m^3$)	$C_b(L)$E+3 ($Kmol/m^3$) Exp.	Model	%Error	$C_p(av)$E+3 ($Kmol/m^3$) Exp.	Model	%Error	% Rej_{av} Exp.	Model	%Error	$F_b(L)$E+4 (m^3/sec) Exp.	Model	%Error
1	5.83	30	0.778	0.856	0.844	1.42	0.375	0.393	-4.80	56.2	53.4	4.98	1.957	2.057	-5.10
2	7.77	30	0.778	0.890	0.882	0.92	0.373	0.3718	0.32	58.1	57.83	0.46	1.86	1.922	-3.33
3	9.71	30	0.778	0.937	0.923	1.49	0.372	0.3687	0.88	60.3	60.04	0.43	1.742	1.788	-2.64
4	11.64	30	0.778	0.984	0.967	1.73	0.37	0.373	-0.81	62.4	61.41	1.58	1.639	1.655	-0.97
5	13.58	30	0.778	1.033	1.014	1.91	0.367	0.3813	-3.89	64.5	62.42	3.22	1.542	1.524	1.16
6	5.83	32	1.556	1.703	1.708	-0.26	0.632	0.698	-10.44	62.9	59.11	6.02	2.01	2.063	-2.63
7	7.77	32	1.556	1.765	1.8	-1.95	0.625	0.628	-0.48	64.6	65.11	-0.78	1.894	1.93	-1.90
8	9.71	32	1.556	1.839	1.903	-3.46	0.618	0.6017	2.63	66.4	68.39	-2.99	1.794	1.799	-0.27
9	11.64	32	1.556	1.926	2.018	-4.73	0.605	0.5938	1.85	68.6	70.58	-2.88	1.684	1.668	0.95
10	13.58	32	1.556	2.023	2.148	-6.14	0.599	0.595	0.66	70.4	72.26	-2.64	1.594	1.538	3.51
11	5.83	31	2.335	2.568	2.54	1.11	0.804	0.853	-6.09	68.7	66.45	3.27	2.022	2.078	-2.81
12	7.77	31	2.335	2.673	2.67	0.12	0.802	0.76	5.23	70	71.35	-1.92	1.907	1.952	-2.35
13	9.71	31	2.335	2.783	2.815	-1.14	0.796	0.732	8.04	71.4	73.98	-3.61	1.815	1.826	-0.60
14	11.64	31	2.335	2.900	2.973	-2.50	0.786	0.722	8.14	72.9	75.7	-3.84	1.707	1.702	0.29
15	13.58	31	2.335	3.035	3.15	-3.78	0.777	0.725	6.69	74.4	76.97	-3.45	1.591	1.579	0.75
16	5.83	31	6.226	6.768	6.71	0.86	1.726	1.82	-5.44	74.5	72.76	2.33	2.082	2.117	-1.68
17	7.77	31	6.226	7.029	7.03	0.00	1.645	1.582	3.82	76.6	77.24	-0.84	1.987	2.004	-0.85
18	9.71	31	6.226	7.287	7.392	-1.43	1.472	1.471	0.06	79.8	80.1	-0.37	1.902	1.89	0.63
19	11.64	31	6.226	7.622	7.787	-2.16	1.433	1.418	1.04	81.2	81.79	-0.72	1.815	1.778	2.03
20	13.58	31	6.226	7.971	8.225	-3.17	1.419	1.395	1.69	82.2	83.02	-0.99	1.734	1.667	3.86

Table 4

Model validation with experimental results for inlet feed flow rate of ($F_b(0)$ =2.583E-4m^3/sec)

No	$P_b(0)$, atm	$T_b(0)$, °C	$C_b(0)E+3$ (Kmol/m³)	$C_b(L)E+3$ (Kmol/m³) Exp.	Model	%Error	$C_p(av)E+3$ (Kmol/m³) Exp.	Model	%Error	% Rej_{av} Exp.	Model	%Error	$F_b(L)E+4$ (m³/sec) Exp.	Model	%Error
1	5.83	29.5	0.778	0.850	0.835	1.84	0.359	0.407	-13.37	57.8	51.21	11.40	2.2	2.317	-5.31
2	7.77	29.5	0.778	0.893	0.867	2.95	0.352	0.380	-8.12	60.6	56.14	7.35	2.075	2.182	-5.15
3	9.71	29.5	0.778	0.932	0.9027	3.21	0.347	0.375	-8.06	62.8	58.44	6.94	1.953	2.048	-4.86
4	11.64	29.5	0.778	0.960	0.9398	2.17	0.343	0.377	-10.11	64.3	59.8	6.99	1.838	1.915	-4.18
5	13.58	29.5	0.778	1.008	0.9795	2.91	0.34	0.384	-12.94	66.3	60.74	8.38	1.72	1.783	-3.66
6	5.83	31	1.556	1.698	1.68	1.07	0.591	0.634	-7.27	65.2	62.25	4.52	2.262	2.327	-2.87
7	7.77	31	1.556	1.76	1.756	0.22	0.572	0.564	1.39	67.5	66.86	0.94	2.148	2.196	-2.23
8	9.71	31	1.556	1.825	1.839	-0.76	0.553	0.539	2.53	69.7	70.67	-1.39	2.042	2.065	-1.14
9	11.64	31	1.556	1.909	1.93	-1.06	0.55	0.532	3.25	71.2	72.43	-1.72	1.947	1.936	0.56
10	13.58	31	1.556	1.996	2.031	-1.73	0.549	0.534	2.73	72.5	73.7	-1.65	1.85	1.807	2.32
11	5.83	31	2.335	2.548	2.518	1.18	0.767	0.863	-12.51	69.9	65.73	5.96	2.29	2.337	-2.052
12	7.77	31	2.335	2.657	2.633	0.91	0.752	0.757	-0.69	71.7	71.24	0.64	2.173	2.209	-1.69
13	9.71	31	2.335	2.735	2.759	-0.87	0.744	0.715	3.83	72.8	74.07	-1.74	2.08	2.083	-0.14
14	11.64	31	2.335	2.841	2.898	-2.00	0.733	0.699	4.54	74.2	75.85	-2.22	1.97	1.957	0.65
15	13.58	31	2.335	2.987	3.051	-2.12	0.726	0.697	3.99	75.7	77.15	-1.91	1.868	1.833	1.87
16	5.83	32	3.891	xx	4.204	xx	xx	1.43	xx	xx	65.98	xx	xx	2.347	xx
17	7.77	32	3.891	xx	4.403	xx	xx	1.218	xx	xx	72.33	xx	xx	2.223	xx
18	9.71	32	3.891	4.504	4.625	-2.68	1.126	1.123	0.26	75	75.71	-0.94	2.113	2.099	0.66
19	11.64	32	3.891	4.635	4.869	-5.02	1.108	1.076	2.88	76.1	77.9	-2.36	2.07	1.976	4.54
20	13.58	32	3.891	4.831	5.141	-6.39	1.092	1.054	3.47	77.4	79.5	-2.71	1.972	1.854	5.98
21	5.83	31	6.226	6.733	6.655	1.16	1.845	1.854	-0.48	72.6	72.15	0.61	2.337	2.374	-1.60
22	7.77	31	6.226	6.977	6.943	0.49	1.549	1.57	-1.35	77.8	77.38	0.53	2.253	2.26	-0.31
23	9.71	31	6.226	7.213	7.261	-0.65	1.486	1.441	3.02	79.4	80.14	-0.93	2.17	2.145	1.15
24	11.64	31	6.226	7.497	7.608	-1.47	1.387	1.377	0.72	81.5	81.9	-0.49	2.09	2.031	2.78
25	13.58	31	6.226	7.794	7.991	-2.52	1.325	1.345	-1.50	83	83.17	-0.20	2.012	1.918	4.67

Note: (xx) means the experimental data have not been reported

6. The effect of operating parameters on the performance of membrane

6.1 The inlet feed flow rate

In this section, the model validated in section 5 is used to investigate the effect of a number of operating parameters on the performance of the process at steady state conditions.

In particular, the feed flow rate is reduced along the membrane channel as can be viewed in Fig. 2 and this can be attributed to the permeated water passing through the membrane which reduces the velocity of feed and increases the brine concentration along the membrane (Fig. 3). It seems that the concentration of feed progresses in the subsequent sub-sections of feed channel since the solute is retained in the wall with the diffusion of water through the membrane. In addition, increasing feed flow rate results in increasing the mass transfer coefficient and decreasing the concentration polarization. This will decrease the solute concentration gradient along the membrane (Fig. 3). A similar trend was observed for all the sets of inlet feed flow rates by Sundaramoorthy et al. (2011b).
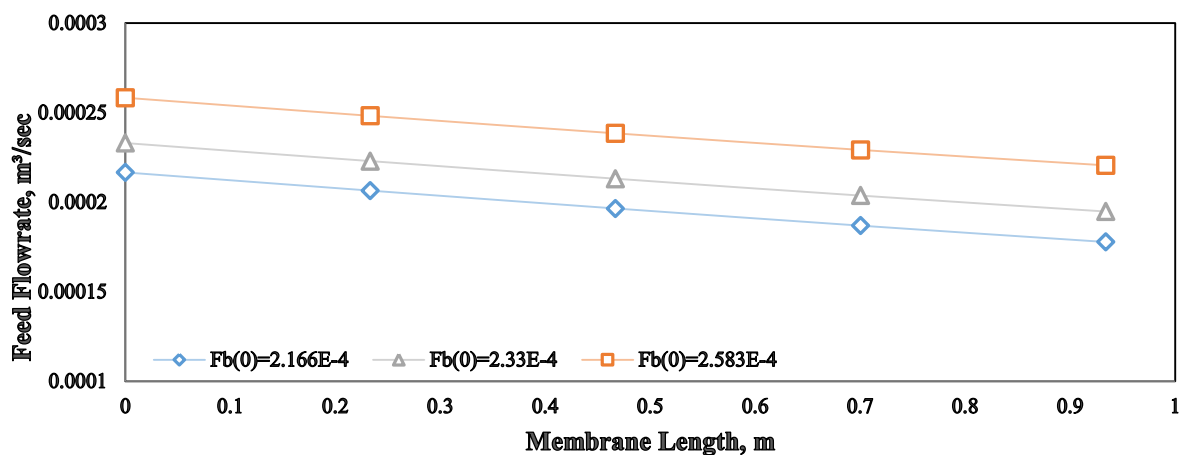
Fig. 2: Steadystate feed flow rate along the membrane length ofdifferent inlet feed flow rates (inlet feed conditions,2.335E-3$kmol/m^3$,7.77 $atm$and 32°C)
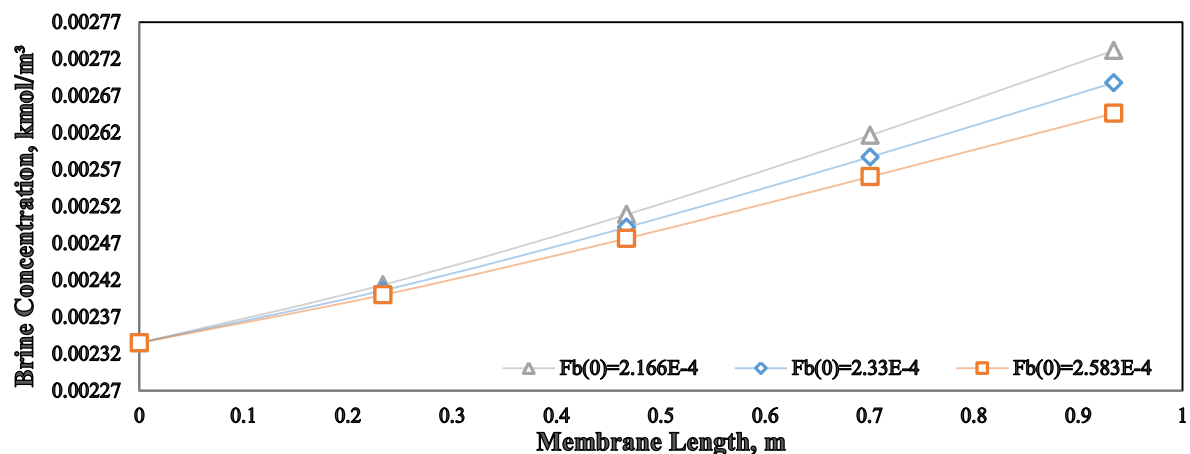
Fig. 3: Steadystate feed concentration along the membrane length of different inlet feed flow rates (inlet feed conditions,2.335E-3$kmol/m^3$, 7.77$atm$and 32 °C)

16

In general, the pressure decreases along the membrane due to friction along the channel length, which decreases the net pressure driving force$(\Delta P_b - \Delta\pi)$ and brings down the diffusion rate of water through the membrane as can be seen in Fig. 4. Also, according to Eq. (2) which describes the water flux, increasing feed pressure increases the permeated water by raising up the trans-membrane pressure ΔP_b above the osmotic pressure $\Delta\pi$.
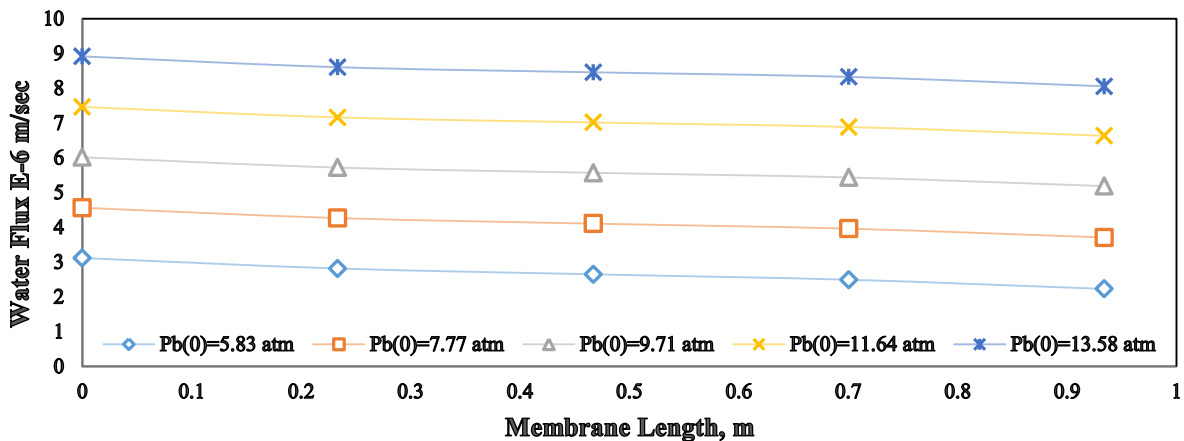
Fig.4: Steadystate water flux along the membrane length ofdifferent inlet feed pressures (inlet feed conditions, 2.583E-4m^3/sec,6.226E-3$Kmol/m^3$and 31°C)

It is usual expectation that increasing inlet feed flow rate would increase the total permeated water, since this would reduce the concentration polarization impact. Surprisingly, at any inlet pressure, increasing feed flow rate has a little influence on the total permeated flow rate (Fig. 5) and no reasonable decrease of water flux (Fig.6). In general, Fig. 6 can be used to better assess the impact of increasing feed flow rate on reducing the concentration polarization (especially in the inlet region of the membrane) which somehow enhances the water flux through the membrane. However, this impact reduces from the middle to the end of the membrane. In addition, %total water recovery along the membrane length decreases as the level of inlet feed flow rates increases (Fig. 7). This event can be attributed to high frictional pressure drop which outweighed the gain of osmotic pressure reduction in each point along the membrane length. Hence, it will create a low driving force and decrease the residence time of feed inside the unit for the flow of fresh water. For this reason, %total water recovery will slightly decrease with increasing inlet feed flow rate under approximately constant total permeated flow rate. Similar results were confirmed by Lee et al. (2010).
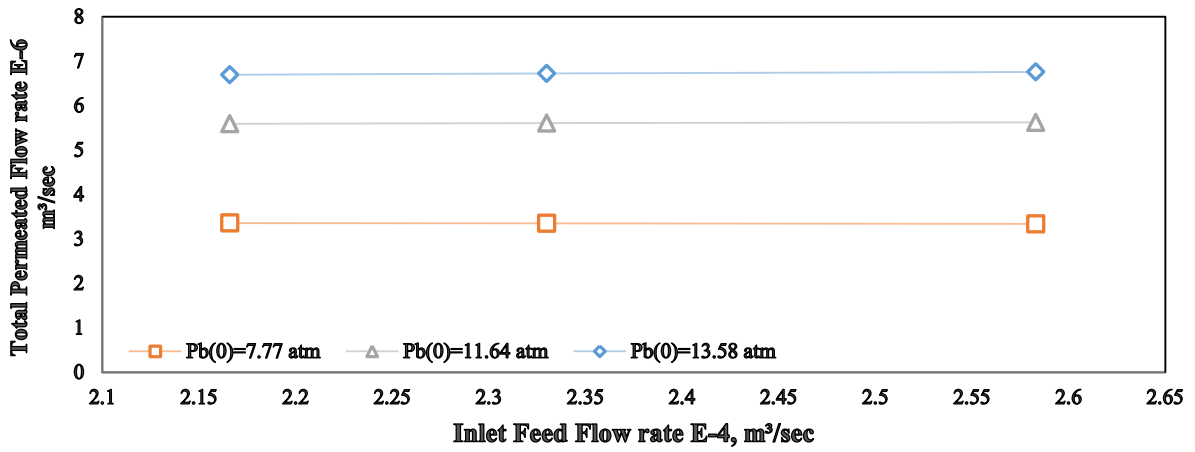
Fig.5: Steadystate total permeated flow rateversusinlet feed flow rateofdifferent inlet feed pressures (inlet feed conditions, 6.226E-3$Kmol/m^3$and 31°C)
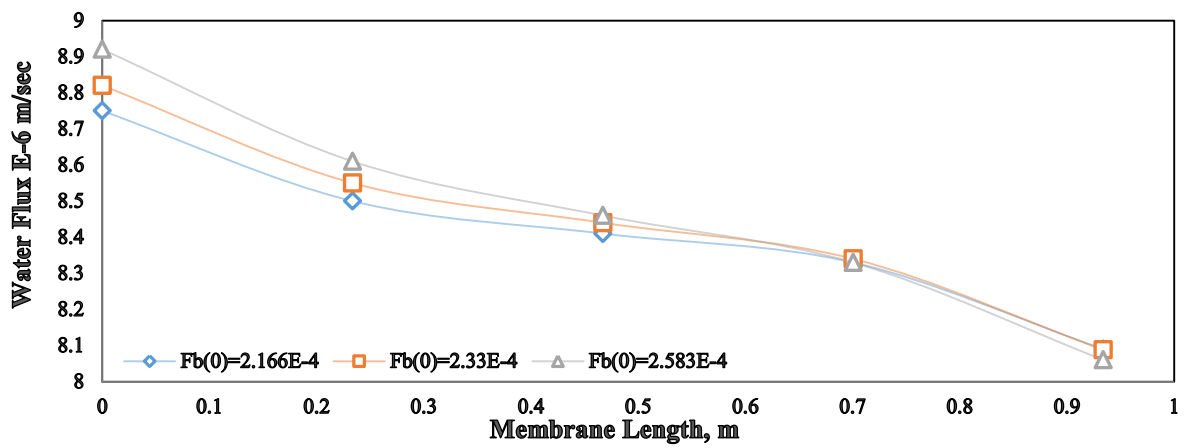

Fig.6: Steadystate water flux along the membrane length of different inlet feed flow rates (inlet feed conditions, 13.58 *atm*, 6.226E-3$Kmol/m^3$and 31°C)
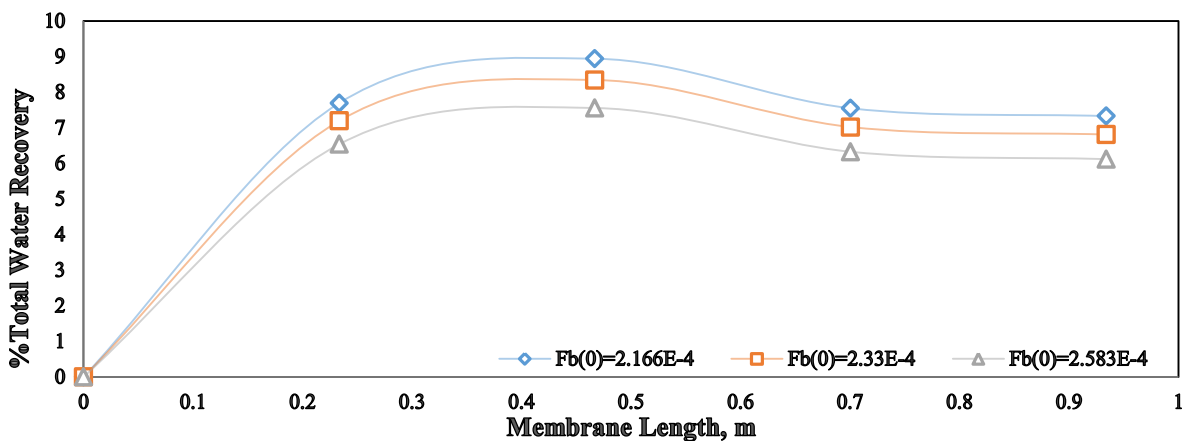
Fig. 7: Steadystate %total water recovery along the membrane length ofdifferent inlet feed flow rates (inlet feed conditions, 6.226E-3$Kmol/m^3$, 13.58 *atm*and 31°C)

On the other hand, increasing inlet feed flow rate reduces the permeate concentration in spite of a slight change inthe permeated water. The reason for this phenomenon is that increasing feed flow rate results in increasing the mass transfer coefficient and decreasing the concentration polarization which is followed by decreasing brine concentration along the membrane. This will lead to a reduction in solute flux,reduction in permeate concentration and increase in %solute rejection (Fig. 8). Furthermore, increasing applied pressure reduces the concentration of the permeated water by increasing water flux.

According to Fig. 8, it can be ascertained that the trend of incline for %solute rejection at high velocities and high pressures conditions is slightly more obvious than at low velocities and low pressures. Thus is because at high velocities, it appears that there is a dispute between the operating variables. Firstly, the mass transfer coefficient increases and the impact of concentration polarization decreases. The greater feed flow rate reduces the wall membrane concentration and causes a decrease of osmotic pressure. However, at the same time, water flux is somewhat decreasing with increasing friction which reduces the quantity of water flux. Consequently, %solute rejection increases as a result of increasing of inlet feed flow rate. In contrast, the trend of %solute rejection at low concentrations (C_b = 1.556E-3 $Kmol/m^3$)(Fig. 9) is more obvious than at high concentrations (C_b = 6.226E-3 $Kmol/m^3$) (Fig. 8). This may be attributed to lower impact of concentration polarization at low feed concentrations which increases the mass transfer coefficient and the total permeated water. These observations are in line with the experimental data of Sundaramoorthy et al. (2011b).
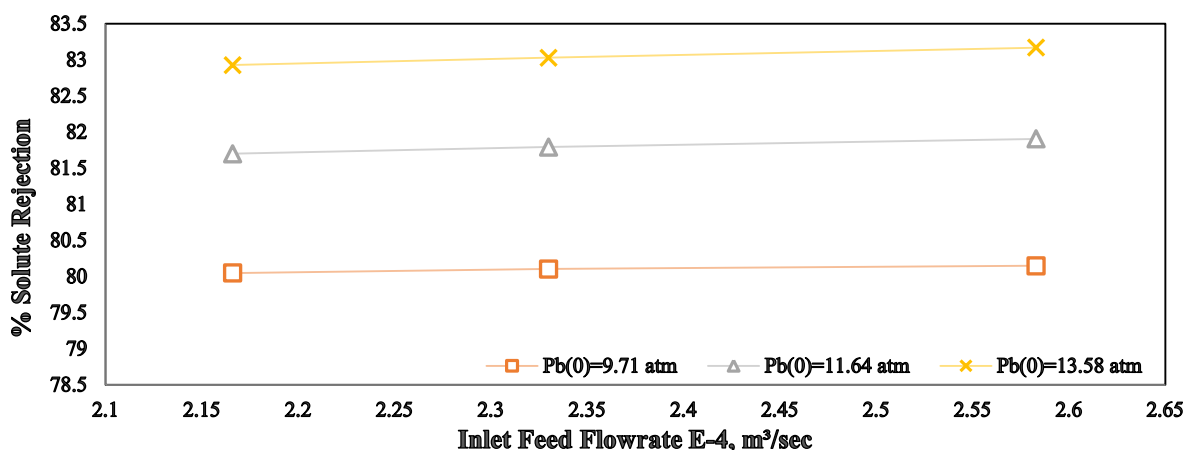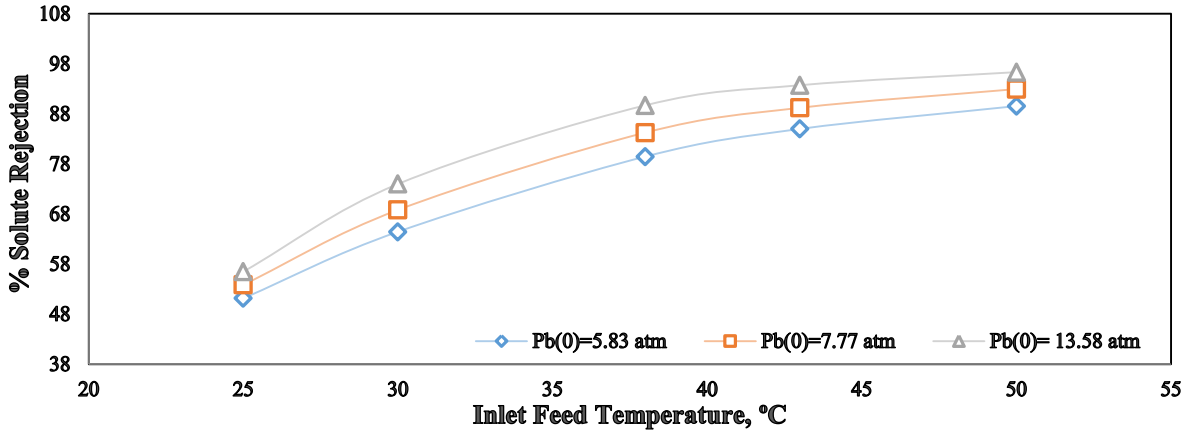

Fig. 8: Steadystate %solute rejection versus inlet feed flow ratesof different inlet feed pressures (inlet feed conditions, 6.226E-3$Kmol/m^3$and 31°C)
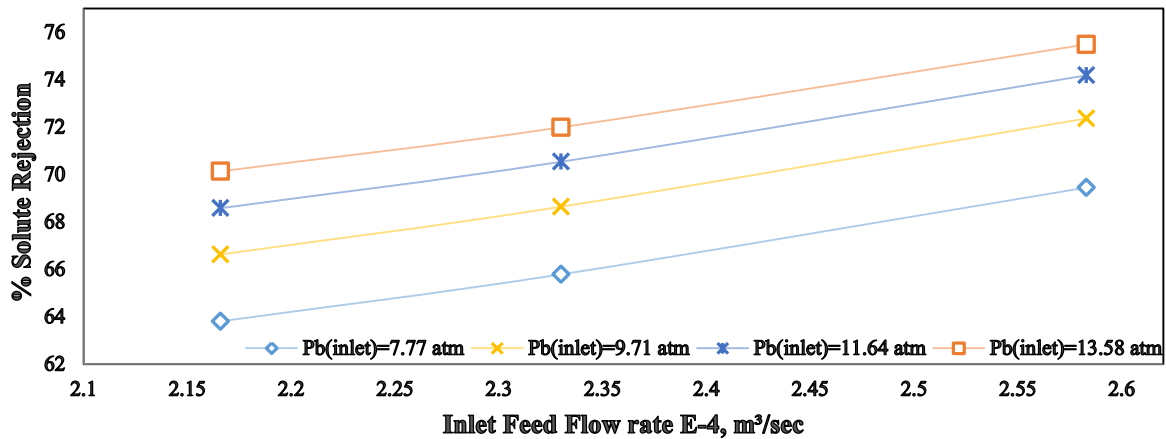
Fig. 9: Steadystate %solute rejection versus inlet feed flow ratesof different inlet feed conditions,1.556E-3$Kmol/m^3$and 32°C)

More often than not, an increment in the feed flow rate causes a specific impact on the wall membrane concentration by decreasing the amount of accumulated salt on the membrane wall. Simultaneously, increasing applied pressure for the same inlet feed flow rate will increase the accumulated salt on the membrane by the increase of the permeated water through the membrane.

6.2 The inlet feed pressure

In steady state mode, the pressure decreases along the membrane channel due to pressure drop caused by the friction. As a result, the pressure gradient is at its maximum point at the entrance of membrane and at its minimum point at the end of the unit. In effect, the water flux and %total water recovery increase due to increase in operating pressure (Fig. 10).Also, the feed pressure has a substantial impact on %solute rejection (Fig. 9) by enhancing the quality of permeate and reducing the solute permeate concentration (Fig. 11). On the other hand, increasing inlet feed concentration for any inlet feed flow rate can cause a reduction in %total water recovery (Fig. 10). This can be attributed to increase in the osmotic pressure that decreases the driving force of water flux and reduces the total permeated water through the membrane.
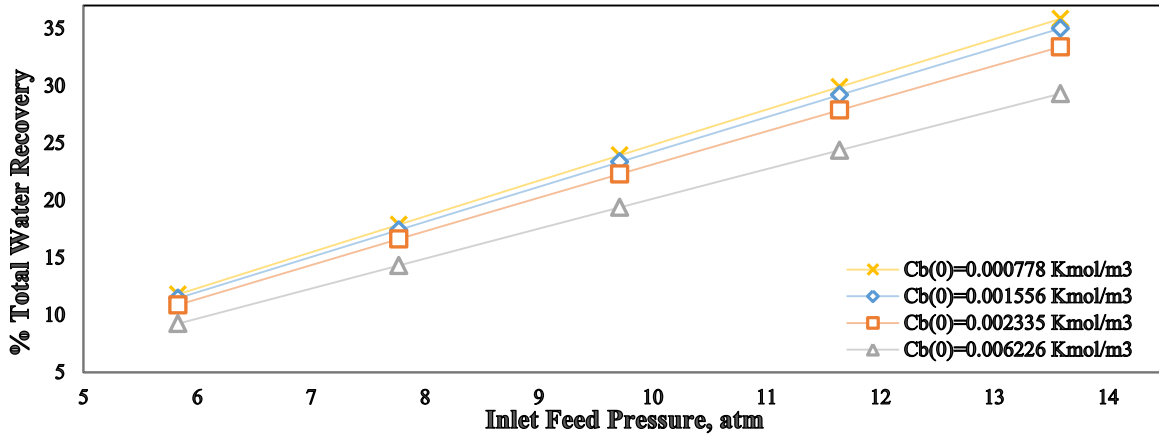
Fig. 10: Steady state %total water recovery versus inlet feed pressures of different inlet feed concentrations (inlet feed conditions, 2.583E-4 m^3/sec and 32°C)
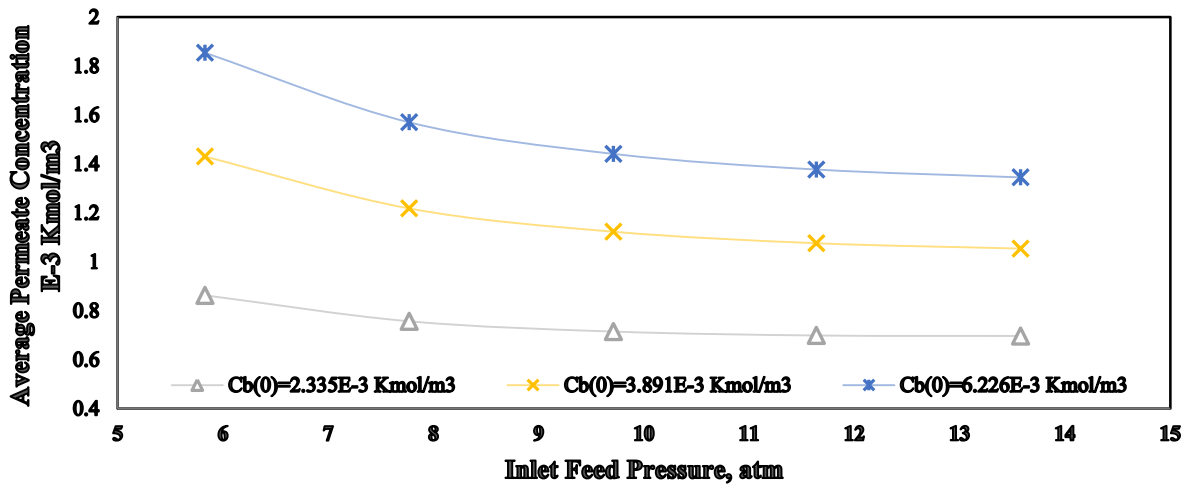
Fig. 11: Steady state average permeate concentrationversus inlet feed pressures of different inlet feed concentrations (inlet feed conditions 2.583E-4 m^3/sec and 32°C)

6.3The inlet feed temperature

Feed water temperature plays an important role in RO process performance. Increasing inlet feed temperature will decrease the viscosity of brine (Eq. 44), which accelerates the flux of water through the membrane and increases %total recovery and %solute rejection in consequence. Another explanation for this trend is that by increasing the feed temperature, the water flux will increase due to the variation of pore size of the polymeric membrane in addition to increase in water diffusivity through the membrane. This fact can be pictured in Fig. 12 for three different feed pressures. According to this figure, it is easy to realize that the temperature has a significant impact on %solute rejection. A similar trend of results has been observed by Mattheus et al. (2002).

Fig.12: Steadystate %solute rejection versusinlet feed temperaturesof different inlet feed pressures (inlet feed conditions, 2.335E-3$Kmol/m^3$and 2.166E-4m^3/sec)

6.4 The inlet feed concentration

The effect of inlet feed concentration on the whole unit can be distinguished through the simulation study. Fig.13 depicts the reduction of water flux along the membrane for increasing inlet feed concentration. This case can be attributed to increase in the osmotic pressure due to increase in the inlet feed concentration which reduces the driving force $(\Delta P_b - \Delta \pi)$ for mass transfer and then reduces the water flux along the membrane. As a result, %total water recovery of the whole unit will slightly decrease. These results are consistent with the findings of Kim et al. (2009).

However, %solute rejection increases due to increase in the inlet feed concentration and this may be due to increase in the membrane solute isolation intensity. The membrane %solute rejection intensity defined in Eq. (56) along the membrane channel shows this fact (Fig. 14).

% Solute Rejection Intensity $= \frac{C_{b(x)} - C_{p(x)}}{C_{b(x)}} x100$ (56)

The %solute isolation intensity is at its maximum value at the beginning of the membrane and at its minimum at the end of the membrane. Likewise, the drop of wall membrane concentration along the membrane can reinforce this case. Finally, all these reasons may explain the effect of inlet feed concentration on %solute rejection (Fig. 15). In addition, increasing operating pressure results in increased %solute rejection. The same results have been confirmed by Avlonitis et al. (1993).
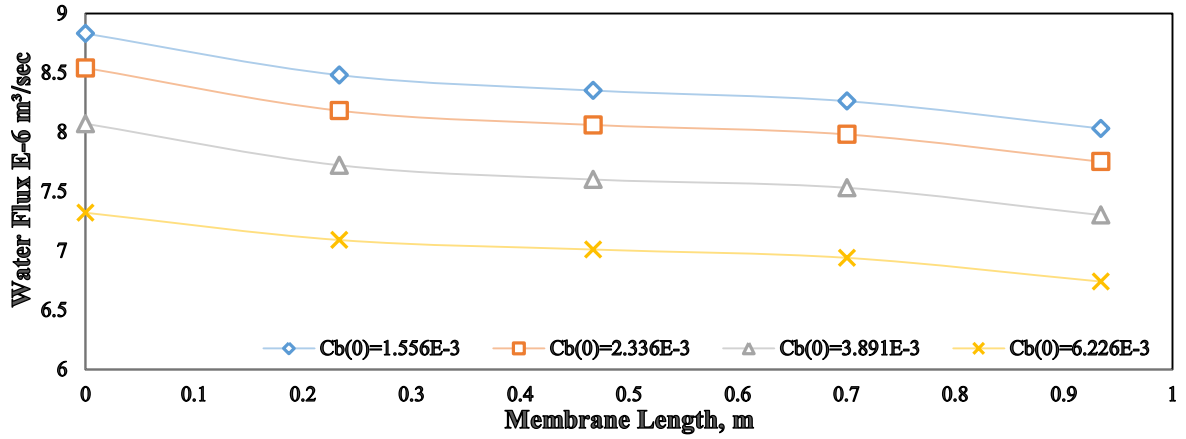
Fig. 13: Steadystate water flux along the membrane length ofdifferent inlet feed concentrations (inlet feed conditions, 2.166E-4 m^3/sec, 11.64 atm and 31°C)

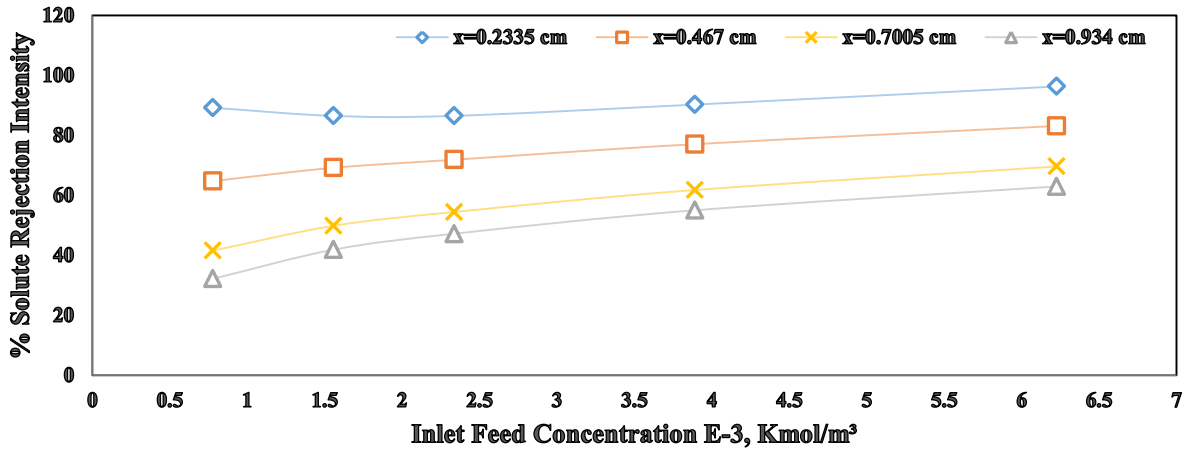Fig.14: Steadystate membrane %solute rejection intensity versusinlet feed concentrationsofdifferent points along the membrane length (inlet feed conditions,2.166E-4 m^3/sec, 11.64 atm and 32°C)

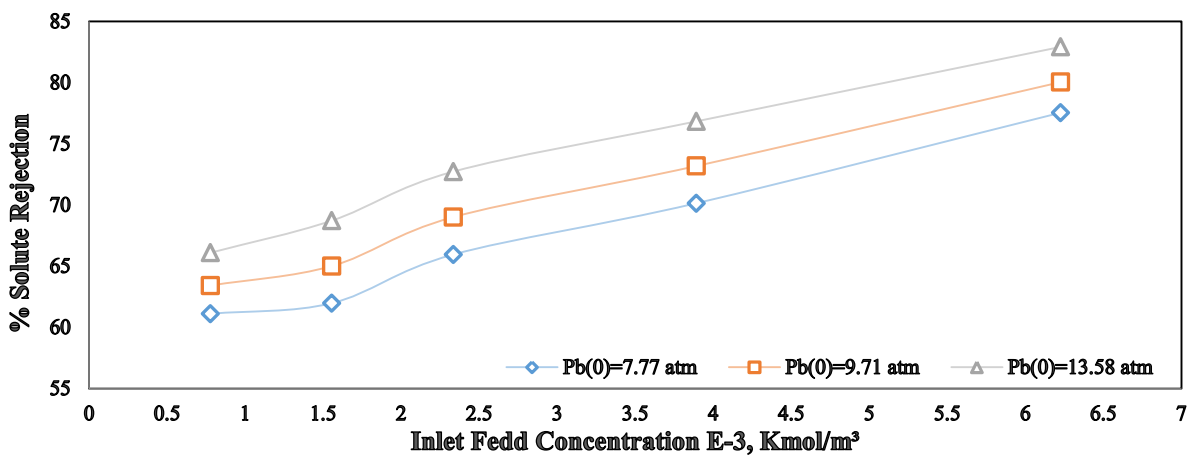Fig. 15: Steadystate %solute rejection versus inlet feed concentrationsof different inlet feed pressures (inlet feed conditions, 2.166E-4 m^3/sec and 31°C)

7. Dynamic simulation

Here, the dynamic model is used to simulate the process and to see the sensitivity of the model to different process parameters. The degree of freedom analysis is presented in appendix A and the input data is shown in Table A.3.

7.1 Effect of inlet feed pressure

The simulation of the dynamic model is carried out by implementing step changes in various parameters.Figs. 16 and 17 show the effectof step change in the inlet feed pressure on the average permeate concentration and %solute rejection for two different initial feed flow rates with fixed inlet feed concentration and temperature. Up to t = 1800 *sec* the inlet feed pressure was 5.83 *atm* and at t = 1800 *sec*, the inlet feed pressure is changed to 13.58 *atm*.

Fig. 16 shows that increasing inlet feed pressure for both inlet feed flow rates ($F_{b(0)} = 2.33E - 4$ and$F_{b(0)} = 4E - 4 \ m^3$/sec) results in decreasing average permeate concentration due to increase in water flux through the membrane. In fact, pressure increase leads to a higher permeate flux which causes an increase in retentate concentration and decrease in the permeate concentration. Also, the reduction of average permeate concentration is greater for high feed flow rate than the lower ones. This is due to the fact that higher inlet feed flow rate together with higher applied pressure reduce the impact of concentration polarization.Figs. 16 and 17 show that the system becomes stable within ($300 - 400sec$) for the two feed flow rates.

In Fig. 16, note that the setting time for higher feed flow rate is a bit longer than the lower feed flow rate (before and after the step change in pressure) and this is due to fact that higher feed flow rate tends to lower the residence time (for a given volume) and vice versa.
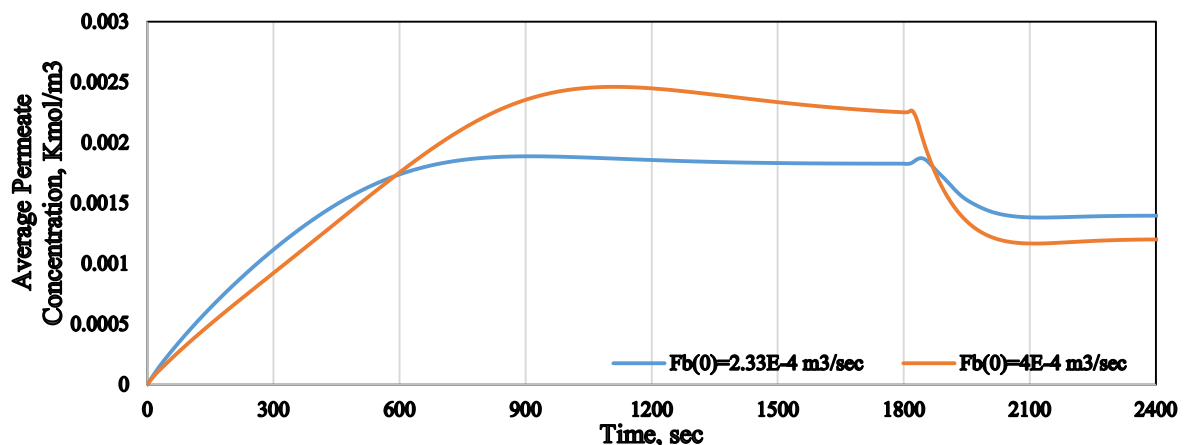
Fig. 16: Impact of step change in inlet feed pressure change on average permeate concentration of different inlet feed flow rates (inlet feed conditions, 6.226E-3$kmol/m^3$and 31°C)
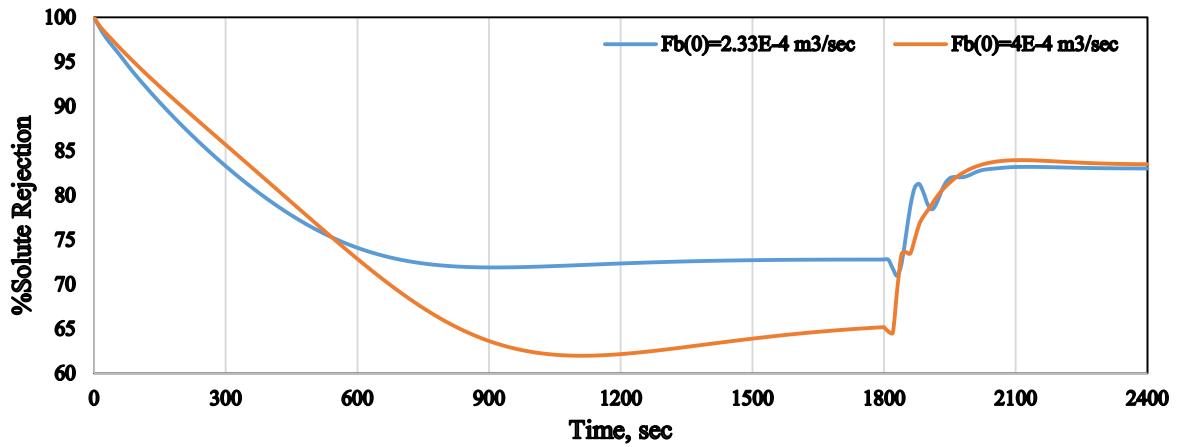

Fig. 17: Impact of step change in inlet feed pressure change on %solute rejection of different inlet feed flow rates (inlet feed conditions, 6.226E-3$kmol/m^3$and 31°C)

For the start-up period (t = 0 to t = 1800 sec), %solute rejection starts at its maximum value when the system works with no concentration polarization. However, the performance of the membrane is retarded due to retained solute along the membrane wall.

Also, Fig. 17 shows that the reduction in %solute rejection for higher inlet feed flow rate is more compared to lower feed flow rate at low pressure step. This is due to increase in the reduction of water flux at higher flow rate that increases the average permeate concentration. However, increasing operating pressure from (5.83 to 13.58 atm) for the two feed flow rates has a similar trend of increasing %solute rejection. Also, it seems that this increase has a significant impact on %solute rejection for the higher feed flow rate in comparison to that by lower feed flow rate. This is due to the fact that higher inlet feed flow rate along with higher applied pressure will improve water flux in comparison to using lower feed flow rate and higher pressure. As a result, %solute rejection of higher feed flow rate will be slightly more than the lower feed flow rate and shows a bigger overshoot.

Additionally, %solute rejection transient response of higher feed flow rate to step change in pressure is insignificant in comparison to lower feed flow rate. This is due to the impact of high pressure and high flow rate conditions which reduces the impact of disturbance in the feed concentration response and reduces the period of feed concentration to arrive at steady state (Fig. 18). Consequently, %solute rejection will be affected by solute concentration response. Also, there is a relatively little overshoot and undershoot in %solute rejection

response to step change in feed pressure at lower feed flow rate before arriving at steady state.

To analyze this behavior, it is crucial to review the dynamic equations of feed and permeate solute concentrations (Eqs. 21 and 22). It can be mentioned that the feed concentration equation has a disturbance variable (feed flow rate) in comparison to output variable (permeated flow rate) in the average permeate concentration equation. It is expected that, increasing inlet feed pressure, temperature and feed flow rate at steady state will affect the feed flow rate directly. Subsequently, the feed concentration will respond to this situation with a fluctuation for a period of time until getting to a new steady value as can be shown in Fig. 20. In contrast, the average permeate concentration response will not be directly affected by this step change   (Fig. 16). However, %solute rejection behavior at the transient time will be somewhat similar to feed concentration trajectory since it comprises the feed and permeate concentrations at channels concurrently (Eq. 30).
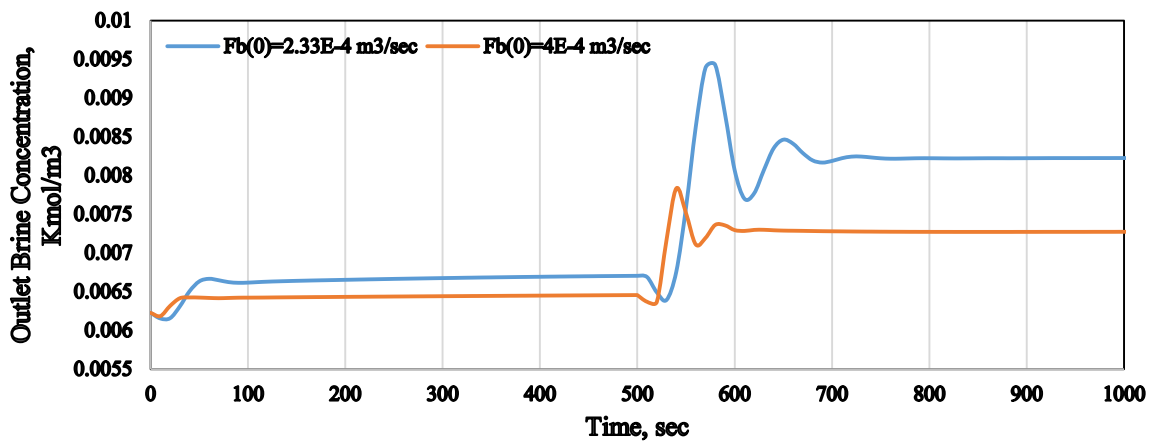

Fig. 18: Impact of step changes in inlet feed pressure on outlet brine concentrationof different inlet feed conditions, 6.226E-3 $kmol/m^3$ and 31 °C)

7.2 Effect of inlet feed flow rate

Figs. 19 and 20 show the effect of step change in inlet feed flow rate on the average permeate concentration and %solute rejection for two different initial feed pressures with fixed inlet concentration and temperature. For step change 1, up to t = 1000 sec, the inlet feed flow rate was 2.33E-4 m^3/sec and at t = 1000 sec, the inlet feed flow rate is changed to 2.583E-4 m^3/sec. While, for step change 2, up to t = 1500sec the inlet feed flow rate was 2.583E-4 m^3/sec and at t = 1500sec, the inlet feed flow rate is changed to 4.0E-4 m^3/sec.

It is clearly noticed that the system has settled within (250 – 350 *sec*) in case of inlet feed flow rate step changes. Fig. 19 confirms that the reduction of permeate concentration is inversely comparable between low and high inlet feed pressures.
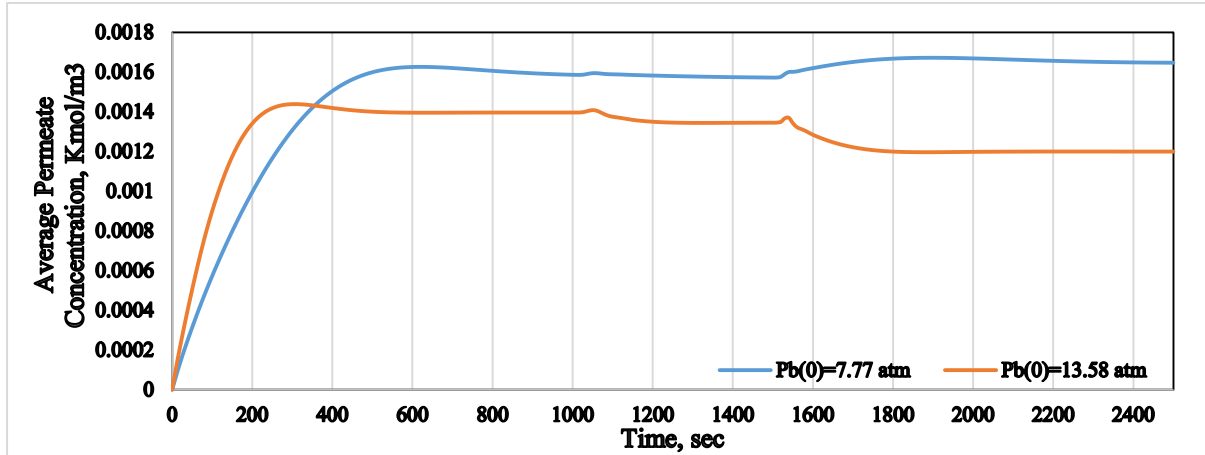

Fig. 19: Impact of step changes in inlet feed flow rate on average permeate concentration of different inlet feed pressures (inlet feed conditions, 6.226E-3 *kmol/m³* and 31 °*C*)

At low inlet pressure, higher inlet flow rates (step change 2) will clearly increase the permeate concentration (Fig. 19). This can be due to the decrease in the residence time in such case, in addition to using low applied pressure ($P_b = 7.7\ atm$). Secondly, increasing inlet feed flow rate results in increasing the frictional pressure drop and thus reducing the gain of osmotic pressure reduction, which finally decreases the quantity of water flux and increases the average permeate concentration. Consequently, %solute rejection will decrease as can be shown in Fig. 20.

In contrast, at high inlet pressure, high inlet feed flow rates (step change 2) result in decrease in the average permeate concentration (Fig. 19). Moreover, the system takes longer time to reach steady state with high inlet feed flow rate in step change 2 in comparison to step change 1. This might be attributed to the increase in the degree of instability during the second step change.
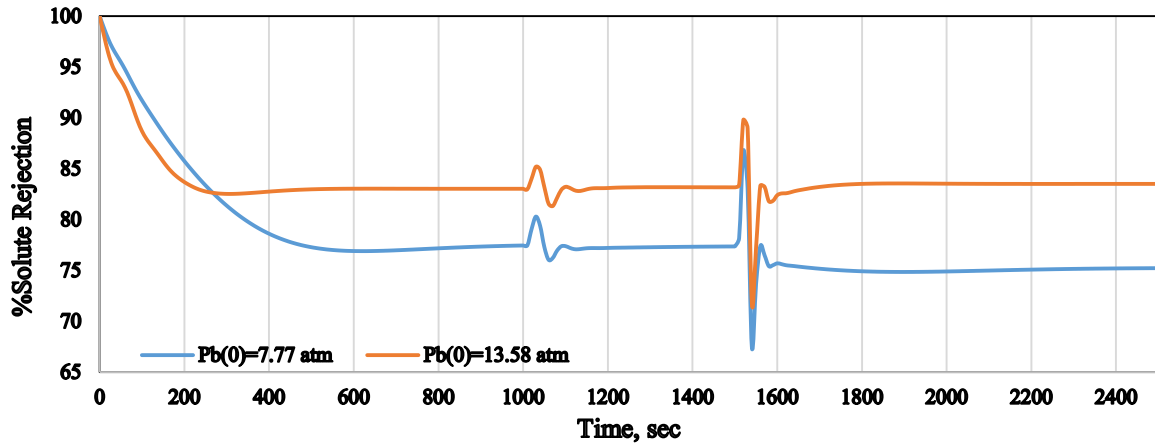
27

Fig. 20: Impact of step changes in inlet feed flow rate on %solute rejection of different inlet feed pressures (inlet feed conditions, 6.226E-3 *kmol/m³* and 31 °*C*)

Once again, the model predicts that the chlorophenol outlet concentration decreases as a result of increase in the inlet feed flow rate for the two step changes. This is due to decrease in the concentration polarization and increase in the mass transfer coefficient with increasing feed flow rate. Finally, this will decrease the solute concentration along the membrane (Fig. 21).
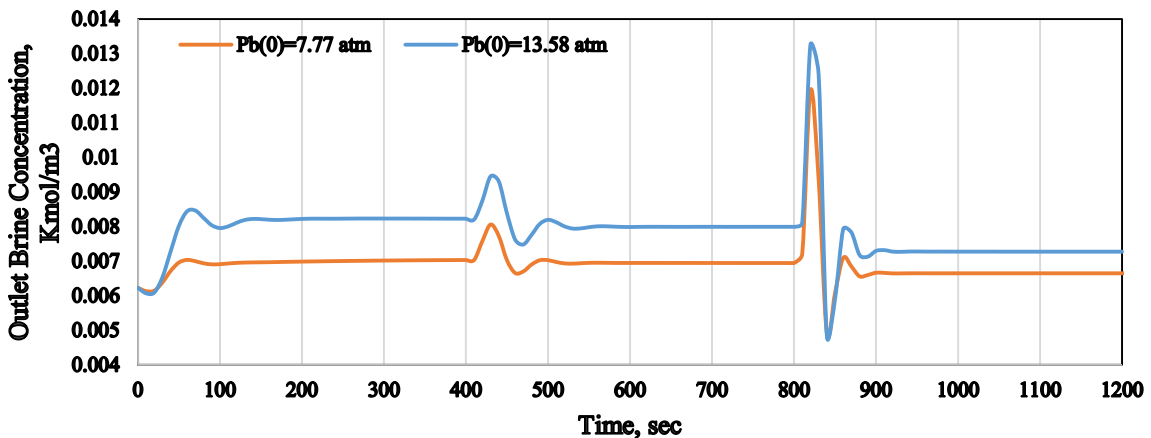

Fig. 21: Impact of step changes in inlet feed flow rate on outlet brine concentration of different inlet feed pressures (inlet feed conditions, 6.226E-3 *kmol/m³* and 31 °*C*)

Fig. 21 shows that the outlet brine concentration undergoes a rapid increase followed by an immediate sharp reduction before getting a new steady state after about 150 sec as a response to the step change in feed flow rate. However, the response is sharper and more rapid (pronounced) for the second step change. It is worthy to mention that the feed concentration

28

at any point along *x-axis* has the same transient response compared to the transient response of the solute concentration at the permeate channel. Moreover, it can be concluded that the average permeate concentration transient response is much slower than the response of the outlet brine concentration.

7.3 Effect of inlet feed concentration

Figs. 22 and 23 show the effectof step change in the inlet feed concentration on the average permeate concentration and %solute rejection for two different initial feed pressures with fixed inlet feed flow rate temperature. For the step change 1, up to t = 1000 *sec*, the inlet feed concentration was 0.778E-3 *Kmol/m³* and at t = 1000 *sec*, the inlet feed concentration is changed to 2.335E-3 *Kmol/m³*. While, for the step change 2, up to t = 2000 *sec*, the inlet feed concentration was 2.335E-3 *Kmol/m³* and at t = 2000 *sec*, the inlet feed concentration is changed to 6.226E-3 *Kmol/m³*.

As expected, increasing inlet feed concentration results in increase in the outlet brine concentration. While, the average permeate concentration increases due to increase in the inlet feed concentration which increases the osmotic pressure (Fig. 22).

Seemingly, the system needs somehow less time to settle in case of high inlet feed pressures in comparison to low feed pressure. Figs. 22 and 23 show that the system needs (500 – 600 sec) to reach a new steady state in the case of using low inlet pressure in both the two step changes. However, the steady state for the high inlet pressure is shorter (300 – 400 sec). This can be attributed to increaseinthe degree of permeation which occurred inside the permeate channel in case of using high pressure.As a result, the water flux increases and reduces the constant average permeate concentration quicker than that obtained using lower values of pressure.
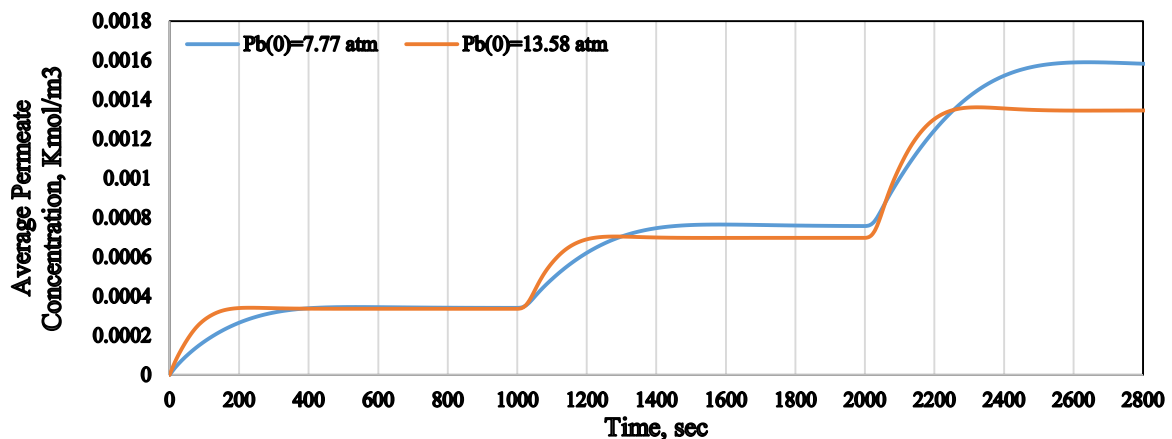
In contrast, %solute rejection increases as result of increasing in the inlet feed concentration due to increase in the intensity of membrane rejection (Fig. 23).
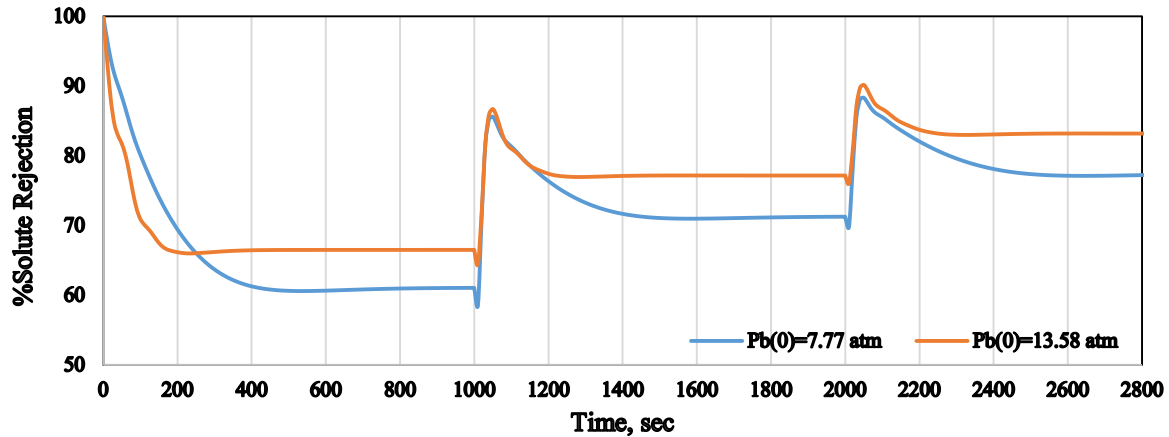

Fig. 23: Impact of step changes in inlet feed concentration on %solute rejection of different inlet feed pressures (inlet feed conditions, 2.583E-4 *m³/sec* and 31 *°C*)

Once again, Fig. 23 shows a little undershoot and clear overshoot for the response of %solute rejection for step changes in feed concentration. The longer shoots can be seen at the first response in comparison to the second response since the first step change is bigger than the second step change. Also, it is expected that these shoots occurred as a consequence of the response of solute concentration on the feed channel (Fig. 21).Moreover, Fig. 23 shows higher %solute rejection with slight undershoot for high pressure in comparison to that by lower pressure. This is due to increase in the water flux as a result of increasing in the applied pressure which lifts up %solute rejection.

7.4 Effect of inlet feed temperature

To investigate the effect of the inlet feed temperature on the performance of the unit, Figs. 24 and 25show the effect of step change in inlet feed temperature on the average permeate concentration and %solute rejection for two different initial feed pressures with fixed inlet feed flow rate and concentration. For the step change 1, up to t = 1000 *sec*, the inlet feed temperature was 27 *°C* and at t = 1000 *sec*, the inlet feed temperature is changed to 35 *°C*. While, for the step change 2, up to t = 2000 *sec* the inlet feed temperature was 35 *°C* and at t = 2000 *sec*, the inlet feed temperature is changed to 43 *°C*.

As expected,increasing inlet feed temperature results inincrease in the solvent viscosity which decreasesthe concentration polarization and increases the water flux. That in turn, will decrease the average permeate concentration (Fig. 24).

It is clearly noted that the system needs (500 – 600 *sec*) to attend steadystate for the two step changes in case of using low inlet feed pressures in comparison to high inlet feed pressure (300 – 400) sec.

Fig. 24: Impact of step changes in inlet feed temperature on average permeate concentration of different inlet feed pressures (inlet feed conditions, 6.226E-3 *kmol/m³* and 2.583E-4 *m³/sec*)

As can be shown in Fig. 25 , the %chlorophenol rejection varies from (74 to 88%) when feed temperature increases from (27 to 35°C) and then increases to 95% at 43°C with 13.58 *atm* inlet feed pressure.
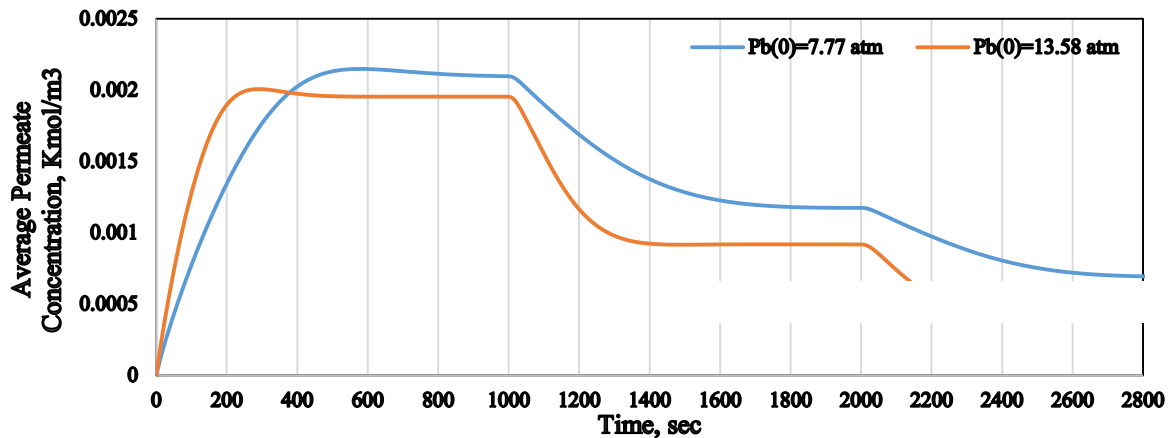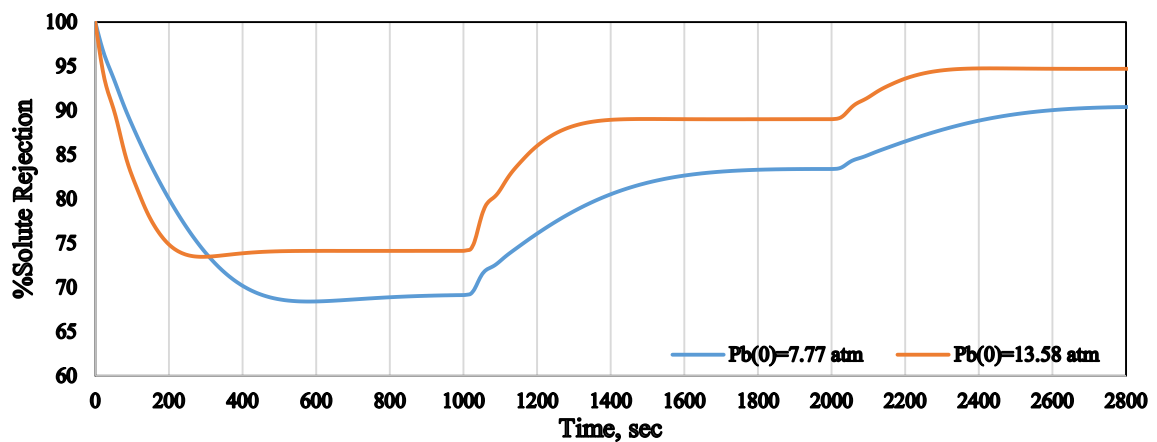

Fig. 25: Impact of step changes in inlet feed temperature on %solute rejection of different inlet feed pressures (inlet feed conditions, 6.226E-3 *kmol/m³* and 2.583E-4 *m³/sec*)

31

8. Conclusions

A mathematical one dimensional steady and dynamic model applicable for dilute binary aqueous solution in a spiral-wound reverse osmosis process has been suggested with a wastewater simulation study. The model can predict the flow rate, concentration, pressure and temperature in each point along the two sides of the membrane length with regard to operating time. Besides, this model can predict the dynamic behavior of water flux, solute flux and solute concentration on the wall of the membrane. A number of explicit differential equations have been suggested for calculating the concentration, pressure, flow rate, temperature with spatial dimensions. Also, the model looks at the impact of concentration, pressure and temperature on the physical properties of the solution resulting in variable mass transfer coefficient and concentration polarization. The model has been validated at steady state conditions against an experimental data of chlorophenol removal and shows accepted relative errors between the theoretical and experimental results for most operating parameters. The model is then used for further simulation to study the impact of various process parameters under steady state and dynamic conditions.

Nomenclature

A_w: Solvent transport coefficient, (*m/atm sec*)

b : Feed and permeate channels friction parameter, (*atm sec/m⁴*)

B_s: Solute transport coefficient, (*m/sec*)

C_b: Brine solute concentration in the feed channel, (*Kmol/m³*)

C_p: Permeate solute concentration in the permeate channel, (*Kmol/m³*)

C_m : Dimensionless solute concentration

C_w : Solute concentration at the membrane wall, (*Kmol/m³*)

D_b: Diffusivity of feed, (*m²/sec*)

D_p: Diffusivity of permeate, (*m²/sec*)

d_{ep} : Equivalent diameter of feed channel, (*m*)

d_{ef} : Equivalent diameter of permeate channel, (*m*)

F_b: Feed flow rate, (*m³/sec*)

F_p: Permeate flow rate, (*m³/sec*)

F_s: Solute molar flux in x-axis, (*Kmol/m² sec*)

J_s: Solute molar flux through the membrane, (*Kmol/m² sec*)

J_w: Water flux, (*m/sec*)

k: Mass transfer coefficient, (*m/sec*)

L : Length of the membrane, (*m*)

M_{wb} : Molecular weight of brine water, (*Kg/Kmol*)

P_b: Feed pressure, (*atm*)

P_p: Permeate pressure, (*atm*)

R: Gas low constant, $\left(R = 0.082 \frac{atm\ m^3}{K\ Kmol} \right)$

Rec : Water recovery coefficient, (*dimensionless*)

$Rec_{(Total)}$: Total water recovery for the whole unit, (*dimensionless*)

Rej: Solute rejection coefficient, (*dimensionless*)

$Rej_{(av)}$: Average solute rejection coefficient, (*dimensionless*)

Re_b : Feed Reynolds number, (*dimensionless*)

Re_p : Permeate Reynolds number, (*dimensionless*)

T_b: Feed temperature, (*C*)

t_f : Feed spacer thickness, (*mm*)

T_p : Permeate temperature, (*C*)

t_p: Permeate spacer thickness, (*mm*)

W: Width of the membrane, (*m*)

Δx: Length of sub-section, (*m*)

μ_b: Feed viscosity, (*Kg/m sec*)

μ_p : Permeate viscosity, (*Kg/m sec*)

ρ_b : Feed density, (*Kg/m³*)

ρ_p : Permeate density, (*Kg/m³*)

ρ_w : Molal density of water, (*55.56 Kmol/m³*)

References

Avlonitis, S., Hanbury, W. T. and Boudinar, M. B.(1991). Spiral wound modules performance.

An analytical solution, part I. *Desalination,* 81(1–3), 191-208.

Avlonitis, S., Hanbury, W. T.and Boudinar, M. B. (1993). Spiral wound modules performance an analytical solution: Part II.*Desalination,* 89(3), 227-246.

Avlonitis, S. A., Pappas, M. and Moutesidis, K. (2007). A unified model for the detailed investigation of membrane modules and RO plants performance. *Desalination,* 203**,** 218-228.

Barello, M., Manca, D., Patel, R. and Mujtaba, I.M. (2015). Operation and modeling of RO desalination process in batch mode, Computers and Chemical Engineering, doi:10.1016/j.compchemeng.2015.05.022

Bódalo-Santoyo, A., Gómez-Carrasco, J.L., Gómez-Gómez,E., Máximo-Martín,F. and

Hidalgo-Montesinos, A.M. (2003). Application of reverse osmosis to reduce pollutants present in industrial wastewater. *Desalination,* 155(2), 101-108.

Boudinar, M. B., Hanbury, W. T. and Avlonitis, S. (1992). Numerical simulation and optimisation of spiral-wound modules. *Desalination,* 86(3)**,** 273-290.

Carter, N. (2015). Desalination and Membrane Technologies:Federal Research and Adoption Issues. Congressional Research Service, 7-5700, www.crs.gov, R40477

Elhalwagi, M.M. (1992). Synthesis of reverse-osmosis networks for waste reduction,

AlChE J. 38, 1185–1198.

Geraldes, V., Escórcio Pereira, N. and Norberta de Pinho, M. (2005). Simulation and

Optimization of Medium-Sized Seawater Reverse Osmosis Processes with Spiral-Wound Modules. *Industrial & Engineering Chemistry Research,* 44(6), 1897-1905.

Jain, S. and S. K. Gupta (2004). Analysis of modified surface force pore flow model with concentration polarization and comparison with Spiegler–Kedem model in reverse osmosis systems.*Journal of Membrane Science,* 232(1–2), 45-62.

Kim, S., Oh, S., Lee, Y., Jeon, M., Kim, I. and Kim, J. (2009). A control methodology for the feed water temperature to optimize SWRO desalination process using genetic programming. *Desalination*, 247, 190-199.

Koroneos, C., Dompros, A. and Roumbas, G. (2007). Renewable energy driven desalination systems modelling. *Journal of Cleaner Production,* 15**,**449-464**.**

Lee, C., Chen, Y. and Wang, G. (2010). A dynamic simulation model of reverse osmosis desalination systems. The 5th International Symposium on Design, Operation and Control of Chemical Processes, PSE Asia, Singapore.

Lonsdale, H. K., Merten, U. and Riley, R. L. (1965). Transport properties of cellulose acetate osmotic membranes. *Journal of Applied Polymer Science,* 9**,** 1341-1362.

Manenti, F., Nadezhdin, I.S., Goryunov, A.G., Kozin, K.A. Baydali, S.A., Papasidero, D., Rossi, F. andPotemin, R. V. 2015. Operational Optimization of Reverse Osmosis Plant Using MPC. Chemical Engineering Transactions, 45, 247- 252.

Mattheus, F. A. Goosen, Sablani, Shyam S., Al-Maskari, Salha S., Al-Belushi, Rashid H. and Wilf, Mark (2002). Effect of feed temperature on permeate flux and mass transfer coefficient in spiral-wound reverse osmosis systems. *Desalination,* 144(1–3), 367-372.

Moonkhum, M., Lee, Y. G., Lee, Y. S. and Kim, J. H. 2010. Review of seawater natural organic matter fouling and reverse osmosis transport modeling for seawater reverse osmosis desalination. Desalination and Water Treatment, 15, 92-107.

Mujtaba, I. M. (2012). The Role of PSE Community in Meeting Sustainable Freshwater Demand of Tomorrow's World via Desalination., In Computer Aided Chemical Engineering- 31, I.A. Karimi and Rajagopalan Srinivasan (Editors), (Editors), Vol 31, pp91-98, Elsevier.

Nguyen, V. T., Vigneswaran, S., Ngo, H. H., Shon, H. K. and Kandasamy, J. (2009). Arsenic removal by a membrane hybrid filtration system. *Desalination,* 236(1–3), 363-369.

Process System Enterprise Ltd., (2001). *gPROMS Introductory User Guide.* London: Process System Enterprise Ltd.

Sagne, Camille, Fargues, Claire, Broyart, Bertrand, Lameloise, Marie-Laure and Decloux, Martine (2009). Modeling permeation of volatile organic molecules through reverse osmosis spiral-wound membranes. *Journal of Membrane Science,* 330(1–2), 40-50.

Sassi, Kamal M. and Mujtaba, Iqbal M. (2012). Effective design of reverse osmosis based desalination process considering wide range of salinity and seawater temperature.*Desalination,* 306(0), 8-16.

Sassi, Kamal M. and Mujtaba, Iqbal M. (2013a). MINLP based superstructure optimization for boron removal during desalination by reverse osmosis. *Journal of Membrane Science,* 440(0), 29-39.

Sassi, Kamal M. and Mujtaba, Iqbal M. (2013b). Optimal Operation of RO System with Daily Variation of Freshwater Demand and Seawater Temperature, Computers & Chemical Eng, 59 (2013) 101–110.

Senthilmurugan, S., Ahluwalia, A. and Gupta, S. K. (2005). Modeling of a spiral-wound module and estimation of model parameters using numerical techniques. *Desalination,* 173(3)*,* 269-286.

Sirkar, Kamalesh K., Dang, Phuong T. and Rao, Goruganthu H. (1982). Approximate design equations for reverse osmosis desalination by spiral-wound modules. *Industrial & Engineering Chemistry Process Design and Development,* 21(3), 517-527.

Slater, C. S., Ahlert, R. C. and Uchrin, C. G. (1983). Applications of reverse osmosis to complex industrial wastewater treatment. *Desalination,* 48(2), 171-187.

Sundaramoorthy, S., Srinivasan, G. and Murthy, D. V. R. (2011a). An analytical model for spiral wound reverse osmosis membrane modules: Part I — Model development and parameter estimation. *Desalination,* 280(1–3), 403-411.

Sundaramoorthy, S., Srinivasan, G. and Murthy, D. V. R. (2011b). An analytical model for spiral wound reverse osmosis membrane modules: Part II — Experimental validation. *Desalination,* 277(1–3), 257-264.

Appendix (A)

Table A.1
The dynamic model equations

No	Title	The Mathematical Expression	Eq.
1	Dynamic axial water flux, m/sec^2	$\dfrac{dJ_{w(x)}}{dt} = \left\{ \left(A_w \left((P_{b(x)} - P_p) - RT_{b(x)}(C_{w(x)} - C_{p(x)}) \right) \right) - J_{w(x)} \right\} \left(\dfrac{F_{b(x)}}{t_f\, W\, \Delta x} \right)$	25
2	Dynamic axial solute flux, $Kmol/m^2\ sec^2$	$\dfrac{dJ_{s(x)}}{dt} = \left\{ \left(B_s\, exp\left(\dfrac{J_{w(x)}}{k_{(x)}} \right)(C_{b(x)} - C_{p(x)}) \right) - J_{s(x)} \right\} \left(\dfrac{F_{b(x)}}{t_f\, W\, \Delta x} \right)$	6
3	Dynamic axial membrane wall concentration, $Kmol/m^3\ sec$	$\dfrac{dC_{w(x)}}{dt} = \left\{ \left(C_{p(x)+}\, exp\left(\dfrac{J_{w(x)}}{k_{(x)}} \right)(C_{b(x)} - C_{p(x)}) \right) - C_{w(x)} \right\} \left(\dfrac{F_{b(x)}}{t_f\, W\, \Delta x} \right)$	27
4	Pressure difference along the membrane, atm	$\Delta P_{b(x)} = (P_{b(x)} - P_p)$	4
5	Dynamic axial feed flow rate, m^2/sec^2	$\dfrac{dF_{b(x)}}{dt} = \left[\left\{ -W \left(A_w \left((P_{b(x)} - P_p) - R\, T_{b(x)}\, exp\left(\dfrac{J_{w(x)}}{k_{(x)}} \right)(C_{b(x)} - C_{p(x)}) \right) \right) \right\} - \dfrac{dF_{b(x)}}{dx} \right] \left(\dfrac{F_{b(x)}}{t_f\, W} \right)$	23
6	Dynamic axial feed pressure, atm/sec	$\dfrac{dP_{b(x)}}{dt} = \left[-b\, F_{b(x)} - \dfrac{dP_{b(x)}}{dx} \right] \left(\dfrac{F_{b(x)}}{t_f\, W} \right)$	24
7	Axial permeated flow rate, m^3/sec	$F_{p(x)} = J_{w(x)}\, W\, \Delta x$	15
8	Dynamic axial molar flux of feed, $Kmol/m^3\ sec$	$\dfrac{dC_{b(x)}}{dt} = -\dfrac{C_{b(x)}}{t_f\, W} \dfrac{dF_{b(x)}}{dx} - \dfrac{F_{b(x)}}{t_f\, W} \dfrac{dC_{b(x)}}{dx} + \dfrac{d}{dx}\left[D_{b(x)} \dfrac{dC_{b(x)}}{dx} \right] - \dfrac{J_{w(x)} C_{p(x)}}{t_f}$	21
9	Dynamic axial molar flux of permeate, $Kmol/m^3\ sec$	$\dfrac{dC_{p(x)}}{dt} = -\dfrac{C_{p(x)}}{t_p\, W} \dfrac{dF_{p(x)}}{dx} - \dfrac{F_{p(x)}}{t_p\, W} \dfrac{dC_{p(x)}}{dx} + \dfrac{d}{dx}\left[D_{p(x)} \dfrac{dC_{p(x)}}{dx} \right] + \dfrac{J_{w(x)} C_{p(x)}}{t_f}$	22
10	Dynamic axial feed temperature, $^oC/sec$	$\dfrac{dT_{b(x)}}{dt} = \left[\dfrac{F_{b(x)}(T_{b(0)} - T_{b(x)})}{t_f\, W\, \Delta x} \right] - \left[\dfrac{J_{w(x)}(T_{b(x)} - T_{p(x)})}{t_f} \right]$	28
11	Dynamic axial permeated temperature, $°C/sec$	$\dfrac{dT_{p(x)}}{dt} = \left[\dfrac{J_{w(x)}(T_{b(x)} - T_{p(x)})}{t_f} \right]$	29
12	Total permeated flow rate, m^3/sec	$F_{p(Total)} = \sum F_{p(x)}$	34
13	Total recovery, *dimensionless*	$Rec_{(Total)} = \dfrac{F_{p(Total)}}{F_{b(0)}}\, X100$	33
14	Average solute rejection, *dimensionless*	$Rej_{(av)} = \dfrac{C_{b(X=L)} - C_{p(av)}}{C_{b(X=L)}}\, X100$	30
15	Average permeated concentration, $Kmol/m^3$	$C_{p(av)} = \sum C_{p(x)}$	31
16	Axial mass transfer coefficient, m/sec	$k_{(x)} de_b = 147.4\, D_{b(x)}\ Re_{b(x)}^{0.13} Re_{p(x)}^{0.739} C_{m(x)}^{0.135}$	54
17	Axial Dimensionless solute concentration, *dimensionless*	$C_{m(x)} = \dfrac{C_{b(x)}}{\rho_w}$	55
18	Axial feed diffusivity, m^2/sec	$D_{b(x)} = 6.725E - 6\, exp\left\{ 0.1546E - 3\, C_{b(x)}\, x18.01253 - \dfrac{2513}{T_{b(x)} + 273.15} \right\}$	42
19	Axial permeated diffusivity, m^2/sec	$D_{p(x)} = 6.725E - 6\, exp\left\{ 0.1546E - 3\, C_{p(x)}\, x18.01253 - \dfrac{2513}{T_{p(x)} + 273.15} \right\}$	43
20	Axial feed viscosity, $Kg\,/m\ sec$	$\mu_{b(x)} = 1.234E - 6\, exp\left\{ 0.0212E - 3\, C_{b(x)}\, x18.0153 + \dfrac{1965}{T_{b(x)} + 273.15} \right\}$	44
21	Axial permeated viscosity, $Kg\,/m\ sec$	$\mu_{p(x)} = 1.234E - 6\, exp\left\{ 0.0212E - 3\ C_{p(x)}\, x18.0153 + \dfrac{1965}{T_{p(x)} + 273.15} \right\}$	45
22	Axial feed density, Kg/m^3	$\rho_{b(x)} = 498.4\, m_{f(x)} + \sqrt{[248400\, m_{f(x)}^2 + 752.4\, m_{f(x)} C_{b(x)}\, x18.0153]}$	46
23	Axial permeated density, Kg/m^3	$\rho_{p(x)} = 498.4\, m_{p(x)} + \sqrt{[248400\, m_{p(x)}^2 + 752.4\, m_{p(x)} C_{p(x)}\, x18.0153]}$	47
24	Axial variable in Equation 45	$m_{f(x)} = 1.0069 - 2.757E - 4\, T_{b(x)}$	48
25	Axial variable in Equation 46	$m_{p(x)} = 1.0069 - 2.757E - 4\, T_{p(x)}$	49
26	Axial feed channel Reynolds number, *dimensionless*	$Re_{b(x)} = \dfrac{\rho_{b(x)} de_b F_{b(x)}}{t_f\, W\ \mu_{b(x)}}$	50
27	Axial permeate channel Reynolds number, *dimensionless*	$Re_{p(x)} = \dfrac{\rho_{p(x)} de_p J_{w(x)}}{\mu_{p(x)}}$	51
28	The equivalent diameter of feed channel, m	$de_b = 2t_f$	52
29	The equivalent diameter of permeated channel, m	$de_p = 2t_p$	53
	Total number of equation is 29		

Table A.2
Specifications of variables

	Total
Variables: $J_{w(x)}, J_{s(x)}, P_{p(x)}, T_{b(x)}, T_{p(x)}, C_{w(x)}, C_{b(x)}, C_{p(x)}, F_{b(x)}, F_{p(x)}, k_{(x)}, F_{p(Total)}, Rec_{(Total)}, Rej_{(av)}, C_{p(av)},$ $de_b, de_p, C_{m(x)}, D_{b(x)}, D_{p(x)}, \mu_{b(x)}, \mu_{p(x)}, \rho_{b(x)}, \rho_{p(x)}, m_{f(x)}, m_{p(x)}, Re_{b(x)}, Re_{p(x)}, \Delta P_{b(x)}, A_w, B_s, L, W, \rho_w, b, P_p, t_f, t_p$ and ρ_w	39
Differential variables at t=0: $\dfrac{dJ_{w(x)}}{dt}, \dfrac{dJ_{s(x)}}{dt}, \dfrac{dC_{w(x)}}{dt}, \dfrac{dF_{b(x)}}{dt}, \dfrac{dP_{b(x)}}{dt}, \dfrac{dC_{b(x)}}{dt}, \dfrac{dC_{p(x)}}{dt}, \dfrac{dT_{b(x)}}{dt}$ and $\dfrac{dT_{p(x)}}{dt}$	9
t is independent variable	1
Total	49

The specification of the dynamic model (Table A.2) shows that the total number of variables is *49*, while the number of equations is *29* as can be seen in Table A.1, so:

D.F. = Total number of variables – Total number of equations

D.F. = 49 – 29 = 20

The number of parameters is 10 (Table A.3) and assigned initial values of differential variables at *t=0* are 9 (Table A.2) and independent variable =1, (time, t). So, this specification counts *20* variables.

Table A.3

Specifications of constant parameters and differential variables at *t=0*

Parameter	Value
Feed spacer thickness (t_f)	0.8 *mm*
Permeate channel thickness (t_p)	0.5 *mm*
Module length (L)	0.934 *m*
Module width (W)	8.4 *m*
Molal density of water, (ρ_w)	55.56 *Kmol/m³*
Gas law constant, (R)	0.082 (*atm m³/°K Kmol*)
Permeate pressure (P_p)	1 *atm*
Feed channel friction parameter, (b)	$8529.45 \left(\frac{atm.sec}{m^4} \right)$
Solvent transport coefficient, (A_w)	$9.5188 \times 10^{-7} \left(\frac{m}{atm.sec} \right)$
Solute transport coefficient, (B_s) (chlorophenol)	$8.468 \times 10^{-8} \left(\frac{m}{sec} \right)$
Differential variables at t=0 $J_{w(0)} = A_w \left(\left(P_{b(0)} - P_p \right) - RT_{b(0)} \left(C_{w(0)} - C_{p(0)} \right) \right)$ $J_{s(0)} = B_s \, exp\left(\dfrac{J_{w(0)}}{k_{(0)}} \right) \left(C_{b(0)} - C_{p(0)} \right)$ $\dfrac{\left(C_{w(0)} - C_{p(0)} \right)}{\left(C_{b(0)} - C_{p(0)} \right)} = exp\left(\dfrac{J_{w(0)}}{k_{(0)}} \right)$ Assigned variables at t=0: $C_{b(0)}, F_{b(0)}, C_{p(0)}, F_{p(0)}, T_{b(0)}$ and $T_{p(0)}$ [These are same as x=0]	